frontiers | Frontiers in Earth Science

ORIGINAL RESEARCH
published: 22 June 2022
doi: 10.3389/feart.2022.920011

Hydrocarbon Generation and Accumulation in the South Junggar Basin, Northwest China: Insights From Basin Modeling

Yuming Liu[1], *Xuesong Lu*[2,3]*, *Mengjun Zhao*[2,3], *Qingong Zhuo*[2,3] *and Lili Gui*[2,3]

[1]China University of Petroleum (Beijing), State Key Laboratory of Petroleum Resources and Prospecting, Beijing, China, [2]China University of Petroleum (Beijing), College of Geosciences, Beijing, China, [3]Key Laboratory of Basin Structure and Hydrocarbon Accumulation, CNPC, Beijing, China

The South Junggar foreland basin (SJFB) is characterized by fold-and-thrust deformation caused by the Cenozoic India–Tibet collision and uplift of the Tianshan Mountains. The tectonic deformation and hydrocarbon accumulation in this region show east-west, north-south, and vertical zoning. Four sets of source rocks are present in the basin, which are middle Permian, Middle–Early Jurassic, Early Cretaceous, and Paleogene in age. The various source rocks are vertically stacked and thus form a composite petroleum system. Due to differences in source rock distribution, hydrocarbon generation, and structural trap formation, the accumulation and distribution of oil and gas is spatially variable. In this study, we presented a detailed analysis of hydrocarbon generation and accumulation in the SJFB based on a combined basin modeling work both in 1D, 2D, and 3D single-well 1D modeling with measured temperature, and Ro data provide the suggested parameters, especially heat flow and erosion thickness, and then a simple 3D model was established based on the thickness maps of each formation and previous work on heat flow distribution. After 3D modeling, the results are rechecked with measured data and finally the source rock maturity map is obtained. By using the advanced “Block” function, the 2D modeling of complicated compressional structural sections has been successfully carried out. Four types of burial and thermal evolution history have been classified, which correspond to the different hydrocarbon phase and maturity. The heterogeneous distribution of oil and gas reflects the variable source rock distribution and maturity evolution, relative timing of hydrocarbon generation, and formation of structural traps. The timing of structural trap formation in the second and third row of anticlines was later than the main phase of hydrocarbon generation, which may explain the poor exploration outcomes in the SJFB. The result indicates that Jurassic and Cretaceous formations in the middle segment of the fold-and-thrust belt in the SJFB are the most favorable combination for hydrocarbon accumulations and have high potential for gas exploration.

Keywords: petroleum system, reservoir-forming conditions, hydrocarbon generation, reservoir-forming combinations, South Junggar foreland basin

OPEN ACCESS

Edited by:
Chen Zhang,
Chengdu University of Technology, China

Reviewed by:
Chunxiao Li,
China University of Geosciences (Wuhan), China
Zhengjian Xu,
Chongqing University of Science and Technology, China
Bo Zhang,
University of Alabama, United States

***Correspondence:**
Xuesong Lu
luxs@petrochina.com.cn

Specialty section:
This article was submitted to Structural Geology and Tectonics, a section of the journal Frontiers in Earth Science

Received: *14 April 2022*
Accepted: *09 May 2022*
Published: *22 June 2022*

Citation:
Liu Y, Lu X, Zhao M, Zhuo Q and Gui L (2022) Hydrocarbon Generation and Accumulation in the South Junggar Basin, Northwest China: Insights From Basin Modeling. Front. Earth Sci. 10:920011. doi: 10.3389/feart.2022.920011

1 INTRODUCTION

The South Junggar foreland basin (SJFB), also known as the North Tianshan piedmont thrust belt, is a superimposed, rejuvenated foreland basin controlled by the Himalayan orogeny (Kang, 2003; Jia et al., 2005; Song et al., 2005; Guo et al., 2006). The long history of petroleum exploration in the SJFB began in the 1930s, and several oil fields (Dushanzi, Qigu, Ganhezi, Santai, Hutubi, Kayindike, and Mahe) and oil-bearing structures (Anjihai, Tulugu, Huoerguosi, and Xihu) have been discovered. As such, the SJFB is an important area for oil and gas exploration in the Junggar Basin (Kang, 2003; Kuang and Jia, 2005; Da et al., 2006, 2007; Kuang and Qi, 2006) (**Figure 1**). Previous studies have identified several combinations of source rocks, reservoirs, and cap rocks in the basin. Multistage tectonic events and complex structures have affected the hydrocarbon accumulation processes and characteristics of the foreland basin (Kuang and Qi, 2006; Guo et al., 2007, 2011; Li et al., 2009), which has limited the success of exploration in the basin.

A comparison of the Mesozoic–Cenozoic sedimentary systems and Cenozoic structures in the North and South Tianshan suggested that the SJFB (North Tianshan) and Kuqa foreland basin (South Tianshan) have comparable source–reservoir–cap rock assemblages and structural traps (Kuang and Liu, 2001; Kang, 2003; Jia et al., 2005; Guo et al., 2007; Li et al., 2010). However, the exploration results in the two foreland basins are quite different. Multiple large gas fields have been successively found in the Kuqa foreland basin, which contains over 1×10^{12} m^3 of gas reserves (Jia et al., 2005; Du et al., 2012; Zhao et al., 2015). However, in the SJFB, much smaller oil and gas reserves have been found, despite the presence of large traps. As such, it remains uncertain as to whether there are any large oil and gas reservoirs in the SJFB and, if present, where such reservoirs might be found.

In this study, we presented a detailed analysis of hydrocarbon generation and accumulation in the SJFB based on a combined basin modeling work both in 1D, 2D, and 3D, including the different burial and hydrocarbon generation histories in different regions, the effective distribution, and the contribution of the four sets of source rock to oil and gas reservoirs. The significant control of source rock maturity and hydrocarbon generation center on hydrocarbon accumulation is revealed. The result indicated that Jurassic and Cretaceous formations in the middle segment of the fold-and-thrust belt in the SJFB are the most favorable combination for hydrocarbon accumulations and have high potential for gas exploration.

2 GEOLOGICAL SETTING

The Cenozoic collision of India and Asia generated compressive stress that has shaped the tectonic framework of the Tianshan Mountains. A series of E–W-trending fold-and-thrust belts have formed in the North and South Tianshan (Molnar and Tapponnier, 1975; Tapponnier and Monlar, 1979; Avouac et al., 1993; Yin et al., 1998; Bullen et al., 2001), which further evolved into a rejuvenated foreland basin (Lu et al., 1994; Lu et al., 2000). In the late Cenozoic, the Tianshan Orogen was rejuvenated, and the fold-and-thrust belts extended farther into the center of the basin, forming structural traps favorable for oil and gas accumulation (Wang et al., 2007; Fang et al., 2007; Jia, 2007, Jia et al., 2008, Jia, 2009; Li B. L. et al., 2011; Xiao et al., 2013). The SJFB is located in the southern Junggar Basin in northwest China and can be divided into a fold-and-thrust belt, a foredeep depression, a northern slope zone, and an uplift zone (from south to north; **Figure 1**). In this study, we mainly consider the fold-and-thrust belt.

2.1 Tectonic Units

The fold-and-thrust belt in the SJFB is located south of the Tianshan and Bogeda mountains, north of the Changji

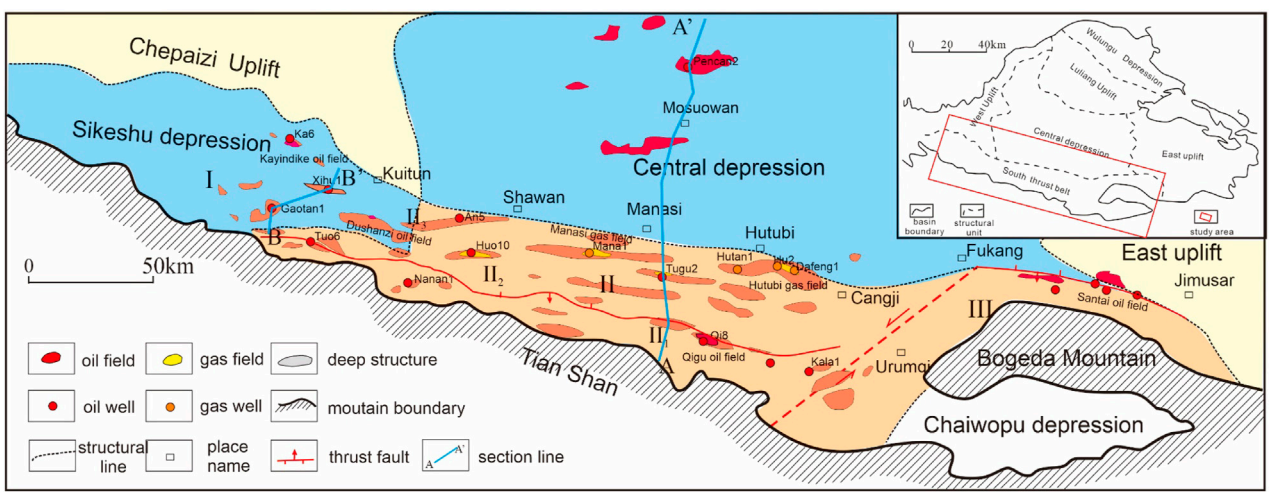

FIGURE 1 | Map showing the structural units and oil–gas fields in the South Junggar foreland basin. The thrust belt is divided into a western segment (I; west to Kuitun), a middle segment (II; between Kuitun and Urumqi), and an eastern segment (III; east to Urumqi). In the middle segment, three en-echelon anticlinal belts strike broadly E–W, that is, the first row of anticlines (II_1), the middle row of anticlines (II_2), and the third row of anticlines (II_3).

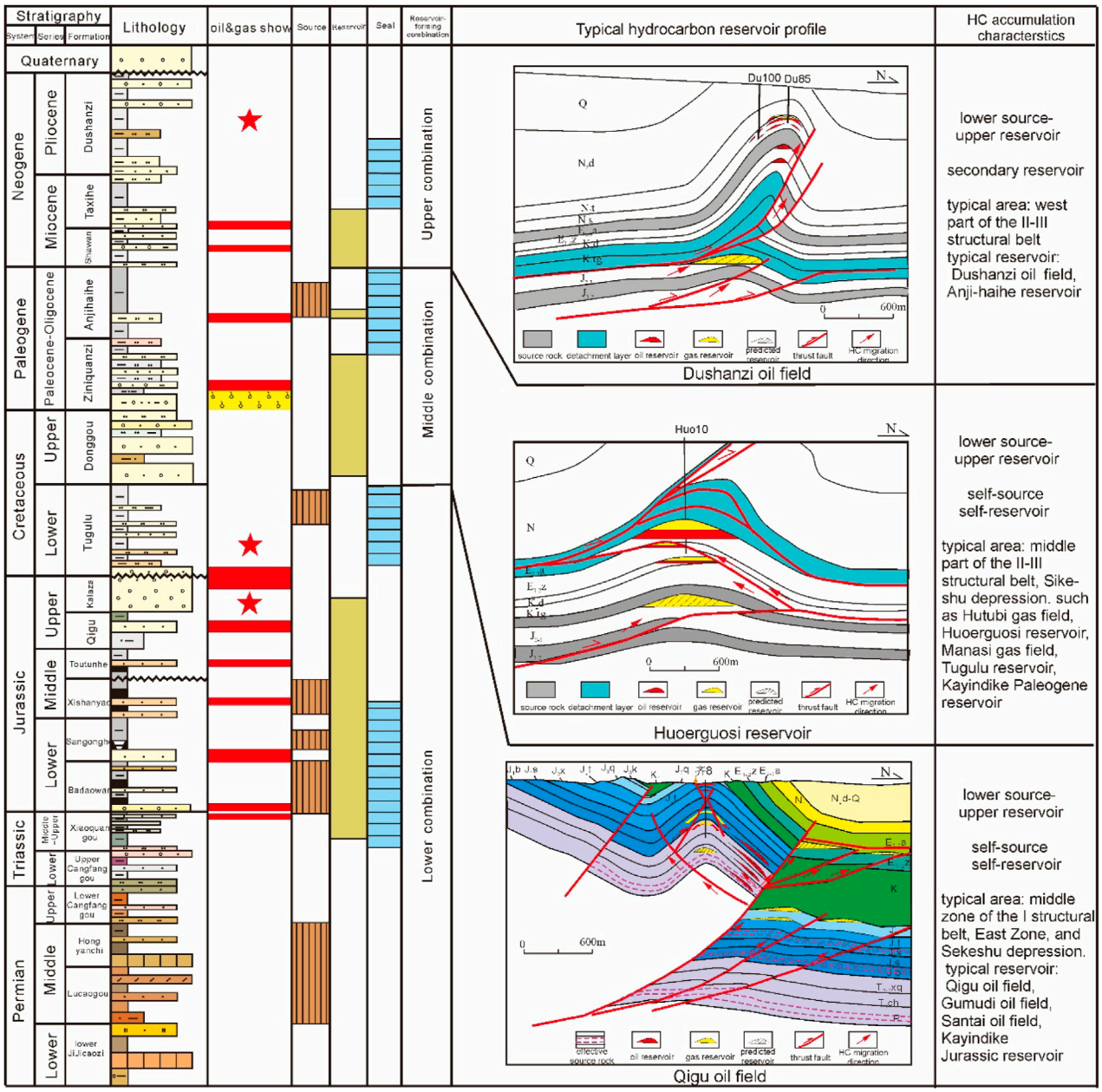

FIGURE 2 | Stratigraphy, hydrocarbon accumulations, and typical cross-sections of oil fields in the South Junggar foreland basin.

depression, east of the Jimusaer depression, and west of the Sikeshu depression. The fold-and-thrust belt is 400 km long and 80 km wide. The tectonic deformation and hydrocarbon accumulation in the belt show obvious east–west, north–south, and vertical changes. In general, the thrust belt is divided into a western segment (I; west to Kuitun), a middle segment (II; between Kuitun and Urumqi), and an eastern segment (III; east to Urumqi) (**Figure 1**). Between the middle and eastern segments, a transverse accommodation zone has been found between Miquan and Changji, which has caused the fold-and-thrust belt to move from west to east and the trend of anticline fold axes to change from WNW–ESE to NE–SW and then back to WNW–ESE.

Three belts of E–W-trending anticlines are presented in the middle segment of the fold-and-thrust belt (**Figure 1**), which comprises fault-related folds such as northward-thrusting, fault-related folds, fault propagation folds, and duplex structures (Burchfiel et al., 1999; Deng et al., 2000; Chen et al., 2010). The first row of anticlines (II_1) includes the Qigu, Kalazha, and Tuositai anticlines. The second row of anticlines (II_2) includes the Dunan, Huoerguosi, Manasi, and Tugulu anticlines. The third row of anticlines (II_3) includes the Xihu, Dushanzi, Anjihai, and

Hutubi anticlines. The fold axes of the anticlines are at a 10°–15° angle to the axis of the North Tianshan thrust faults. The northern limbs of the anticlines are generally steeper than the southern limbs and, from South to North, the lengths of the anticlines decrease. The younger formations are less deformed than the older formations, reflecting continued sedimentation during deformation. All these characteristics suggested that the primary stress is related to the Tianshan Orogen and involves dextral transpressional deformation (Liu et al., 1994; Yu et al., 2009).

2.2 Stratigraphy and Sedimentation

Sedimentation in the SJFB began in the late Paleozoic and formed a complete suite of Permian–Quaternary terrestrial deposits (**Figure 2**). The Permian strata comprised the Jijicao series (P_1j), and the lower Cangfanggou Formation (P_2ch). P_1j is mainly found between Urumqi and Jimusar and is a marine–terrestrial deposit, comprising sandstones, siltstones, and shales–mudstones, interbedded with tuffs, oil shales, and dolomites. P_2ch is widespread in the northern Tianshan and is in unconformable contact with P_1j or Carboniferous rocks. The main lithology of the P_2ch is variegated to purplish-red terrestrial clastic rocks. The Triassic strata include the upper Cangfanggou (T_1ch) and Xiaoquangou formations ($T_{2-3}xq$), which comprise mainly gray mudstones, muddy siltstones, lithic sandstones, and sandy mudstones. T_1ch is a typical braided alluvial–deltaic conglomeratic deposit. The Jurassic strata have the widest and thickest (>4,000 m) distribution in the SJFB. From the base to top, Jurassic rocks include the Badaowan (J_1b), Sangonghe (J_1s), Xishanyao (J_2x), Toutunhe (J_2t), Qigu (J_3q), and Kalazha (J_3k) formations. The lower J_1b consists of gray mudstones interbedded with sandstones, and the upper J_1b consists sandy mudstones interbedded with sandstones, along with thin coal beds and lenses. J_1b is a braided river–shallow lake facies deposit that records a lake transgression. J_1s comprise grayish-green mudstones and sandstones interbedded with thin coal lenses, which were deposited in braided alluvial–deltaic facies. J_2x is the thickest Jurassic formation with local thicknesses of >1,000 m. J_2x consists of grayish-green sandstones and mudstones, interbedded with coal beds or lenses, deposited in a typical swamp facies environment. J_2t comprises variegated mudstones, sandy mudstones, and sandstones that were deposited in braided river facies. In the upper part of J_2t, the formation is red, which shows that the climate was during deposition. J_3q consists of red and purple mudstones interbedded with sandstones. J_3k typically comprises brown and red conglomerates and is often referred to as the Kalazha Dike due to its steep geomorphology. Cretaceous strata include the Tugulu (K_1tg) and Donggou formations (K_2d), which comprise grayish-green mudstones interbedded with sandstones and lower conglomeratic sandstones. A lake regression occurred from the Early to Late Cretaceous. Paleogene strata include the Ziniquanzi ($E_{1-2}z$) and Anjihaihe formations ($E_{2-3}a$). $E_{1-2}z$ comprises mainly purple mudstones and sandstones, and $E_{2-3}a$ consists of variegated mudstones and sandy mudstones interbedded with sandstones. Neogene rocks comprise the Shawan (N_1s), Taxihe (N_1t), and Dushanzi formations (N_2d). N_1s consists of brown muddy siltstones and mudstones with conglomerate interbeds. N_1t comprises brown sandy conglomerates and muddy sandstones. N_2d consists of lower yellow sandy mudstones and upper conglomerates interbedded with sandstones. Quaternary strata are dominated by the Xiyu Formation, which consists of conglomerates with lithic sandstone and sandy mudstone lenses. This entire Permian–Quaternary sedimentary sequence is the foundation of the petroleum system in the SJFB.

2.3 Geological Structure and Tectonic Deformation

The SJFB can be divided into three structural layers controlled by two regional detachments (mudstones in $E_{2-3}a$ and K_1tg) (Guo et al., 2011; Guan et al., 2016): 1) a Miocene–Quaternary structural layer above $E_{2-3}a$; 2) a Paleogene–Cretaceous structural layer between $E_{2-3}a$ and K_1tg; and 3) a pre-Cretaceous structural layer beneath K_1tg. An N–S cross-section in the middle segment of the SJFB both with the seismic section and explained structure and petrography mode shows the vertical stratified structural deformation and the three rows of anticlines (**Figure 3**); from South to North, the anticline are the Qigu anticline and Huoerguosi antilcine, respectively.

The growth strata that developed in fold-and-thrust belts provide the most reliable basis for determining the timing of structural events (Suppe et al., 1992; Shaw and Suppe, 1994). Many studies have used growth strata to determine the timing and rate of tectonic deformation (Wang et al., 2002; Guo et al., 2006; Li et al., 2011b) in the northern and southern Tianshan thrust belt. It has generally been concluded that the first row of anticlines formed in the late Mesozoic acquired its present geometry during the Himalayan orogeny and ceased developing during the Pleistocene (Deng et al., 2000). The second row of anticlines are formed between the Pliocene and early Pleistocene (Deng et al., 2000; Charreau et al., 2008, 2009). Given that the conglomerate in the Xiyu Formation is 2.58 or 3.10 Ma in age (Sun et al., 2004; Charreau et al., 2005), the second row of anticlines must have formed after 3 Ma (Guo et al., 2006; Fang et al., 2007). The third row of anticlines formed after the middle Pleistocene at ca. 0.73 Ma (Zhang et al., 1996; Deng et al., 2000). From east to west and from south to north, the strata and timing of anticline formation become younger, the folding amplitude becomes smaller, and the intensity of deformation decreases (Lu et al., 2010).

2.4 Source Rocks and Petroleum Systems

Based on oil–source correlations and geochemical characteristics, four sets of source rocks have been identified: the middle Permian Lucaogou Formation (P_2l), the Lower–Middle Jurassic (J_{1-2}), K_1tg, and $E_{2-3}a$ (Chen et al., 2015a).

P_2l is widely distributed in the middle and eastern SJFB (**Figure 3**). The average thickness of the Permian source rocks is 250 m, with the depocenter in the Changji–Fukang area. P_2l

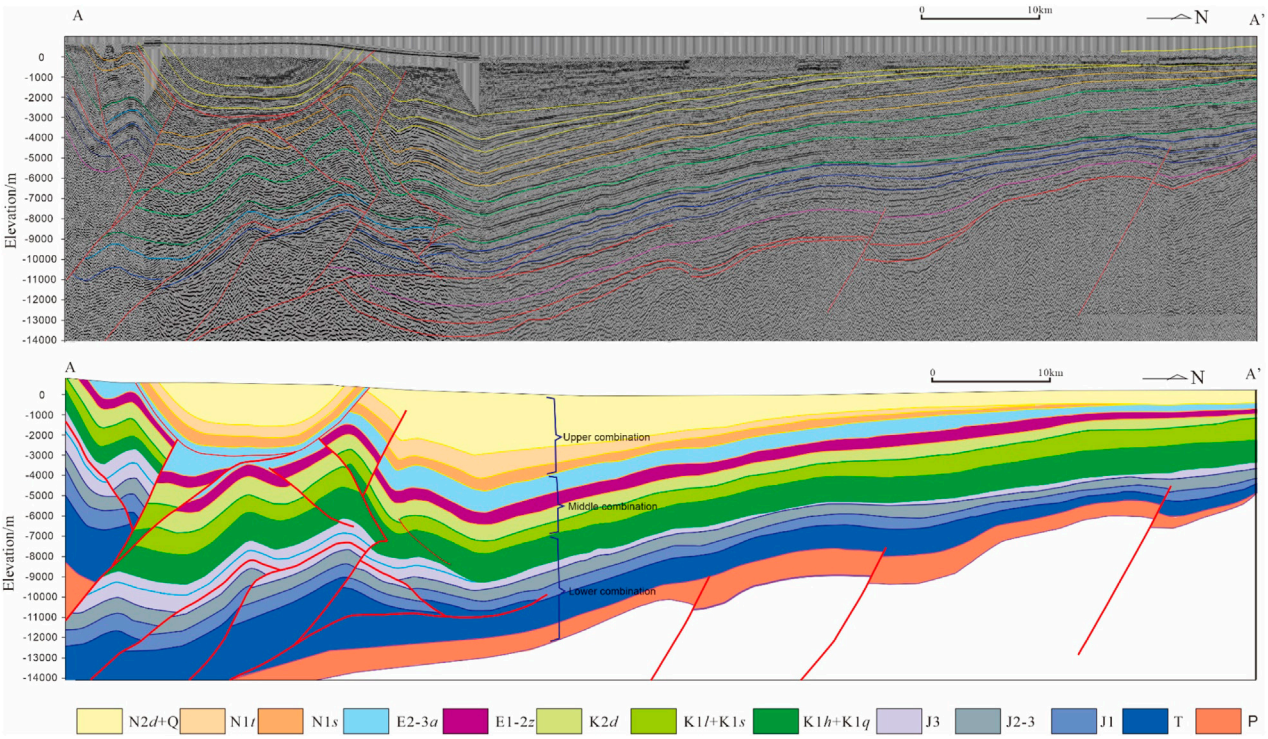

FIGURE 3 | N–S cross-section in the middle segment of the SJFB shows the seismic and structural and stratigraphy characteristics. The location of this section is shown in **Figure 1**. The three sets of combinations can be divided vertically by the regional detachment layer and caprock.

comprises mudstones deposited in a lacustrine facies, with high total organic carbon (TOC) and type I and II_1 organic matter contents. The exposed and drilled rocks of the P_2l are located mainly in the piedmont region of the middle segment (II). In the Yaomoshan outcrop, P_2l is at the low-maturity stage. In the Xiaoquzi area, the Ro values of P_{2l} drilled by the Xiao 1 and Xiao 3 wells are 0.50–0.75%. In the foredeep depression, no Permian source rocks have been drilled, but these should be present at depths of ≥10,000 m and are anticipated to be in the high- to the post-mature stage.

Jurassic source rocks are widely distributed in the SJFB, with an average thickness of 160 m (locally >500 m). These rocks are black carbonaceous mudstones with coal interbeds that formed in a lacustrine–swamp facies. The source rocks are found mainly in J_1b, J_1s, and J_2x. The organic matter type is III and II_2 and mainly generates gas. The Jurassic source rocks are mostly at the low- to the mid-mature stage. However, at the center of the depression, the Jurassic source rocks would be in the high- to the over-mature stage.

Cretaceous source rocks are found mainly in K_1q in the middle (II) and western (III) segments in the Huoerguosi–Manasi–Tugulu areas. The lithology is a deep-water, lacustrine, dark mudstone, with TOC contents of 0.06–1.81%. The organic matter is mainly type I and II (Chen et al., 2015a).

Paleogene source rocks are mainly present in $E_{2-3}a$ in the western Sikeshu depression. These source rocks are shallow to semi-deep, lacustrine facies, and dark gray mudstones, with TOC contents of 0.06–7.55% (average of 1.03%). The organic matter is mainly type II_1 and II_2. The Paleogene source rocks are generally found at shallow depths and are in the immature to the early-mature stage (Chen et al., 2015a).

From the Permian to the Quaternary, the center of deposition and subsidence moved progressively to the west. The four sets of source rocks are vertically stacked and overlap, forming a composite petroleum system. As such, there are four petroleum systems, which are derived from middle Permian, Middle–Lower Jurassic, Lower Cretaceous, and Paleogene source rocks (**Figure 4**). Numerous faults connect the source rocks in the SJFB (**Figures 2**, **3**), resulting in the mixing of hydrocarbons from these different sources (Li et al., 2003; Da et al., 2006, 2007; Li et al., 2007). In the vertical direction, the hydrocarbon reservoirs mostly have mixed sources. In plain view, middle Permian petroleum systems are present in the middle and eastern segment and the Middle–Lower Jurassic petroleum system is distributed broadly in the whole basin. The Lower Cretaceous petroleum system distributes locally in the middle segment. Locally, the Paleogene petroleum system is present in the deeply buried parts of the Sikeshu depression. The existence of four sets of source rocks and different times of hydrocarbon generation and expulsion has formed these complex hydrocarbon accumulations (**Figure 4**).

Oil and source rock geochemistry correlation shows that the oil in the SJFB can be divided into four types (Chen et al., 2015b, 2016), as follows (**Figure 5**).

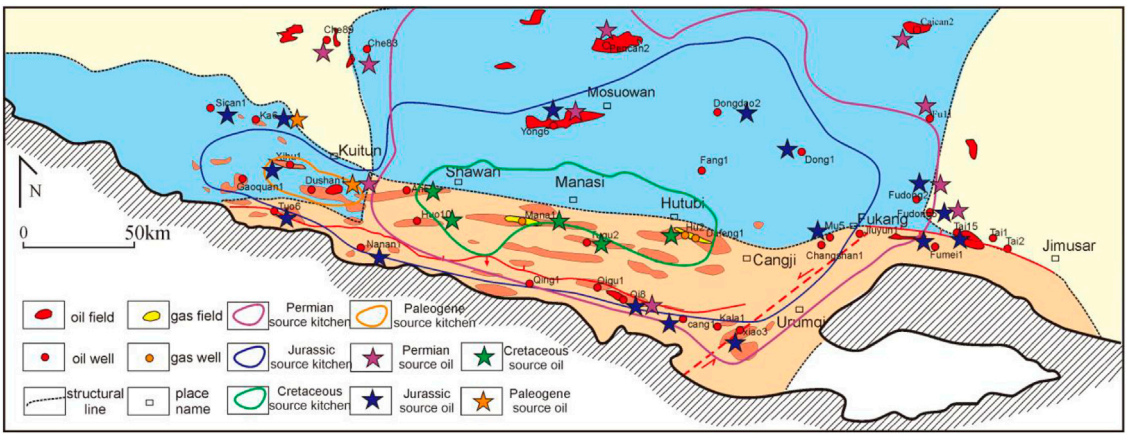

FIGURE 4 | Map showing the distribution of the four sets of effective source rock and four types of oil in the South Junggar foreland basin.

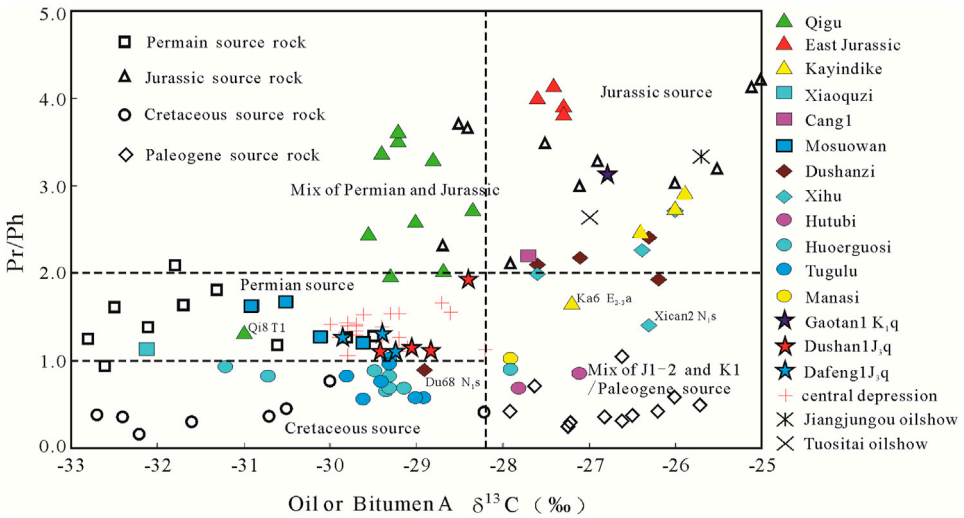

FIGURE 5 | Oil source discrimination diagram based on stable carbon isotope data and Pr/Ph values.

1) Type I: This oil has $\delta^{13}C < -29‰$, Pr/Ph = 1–2, and contains abundant β-carotene, mainly regular sterane with C_{28} and C_{29}, and low abundances of rearranged sterane. This is typicalof Permian source rocks and, as such, it was concluded that Type I oil was sourced from such rocks. Type I oil is found mainly in the eastern segment of the thrust belt, such as in the Qi 8 well and the Xiaoquzi oil field. The oil in the Dushan 1 and Dafeng 1 wells in the middle segment might also be sourced from Permian source rocks, as indicated by carbon isotope and Pr/Ph data (**Figure 5**).
2) Type II: This oil has $\delta^{13}C = -28$ to $-26‰$, Pr/Ph > 2.0, and contains abundant regular sterane and rearranged sterane with C_{29}, which are characteristics of Jurassic source rocks. Type II oil is found mainly in the Xihu and Kayindike oil fields and the Tuositai and Jiangjungou oil seeps in the western segment and in the Gumudi and Santai oil fields in the eastern segment. The Jurassic oil in the Qigu oil field is similar to Type II oil in terms of biomarkers, but the carbon isotopes are heavier, and thus it is concluded that this oil was mixed with oil from Permian source rocks (**Figure 5**).
3) Type III: This oil has $\delta^{13}C = -32$ to $-29‰$, Pr/Ph < 1.0, and contains regular steranes that are mainly C_{27} and C_{29} and isocholestane and abundant rearranged sterane and gammacerane, which are typical of Cretaceous source rocks. The type III oil is present mainly in the second and third rows of anticlinal belts, such as oils in the Neogene and Cretaceous in the Tugulu, Manasi, Huoerguosi, Anjihai, South Anjihai, and Hutubi anticlines.
4) Type IV: This oil has $\delta^{13}C = -28$ to $-25‰$ and contains C_{27} and C_{29} steranes with a "V" shape and abundant 4-methyl-24-ethyl triaromatic cholestane, which is typical of Paleogene source rocks. Type IV oil is found mainly in $E_{2-3}a$ in the Kayindike anticline, N_1t in the Xihu anticline, and N_1t and N_1s in the Dushanzi oil field. A controversy

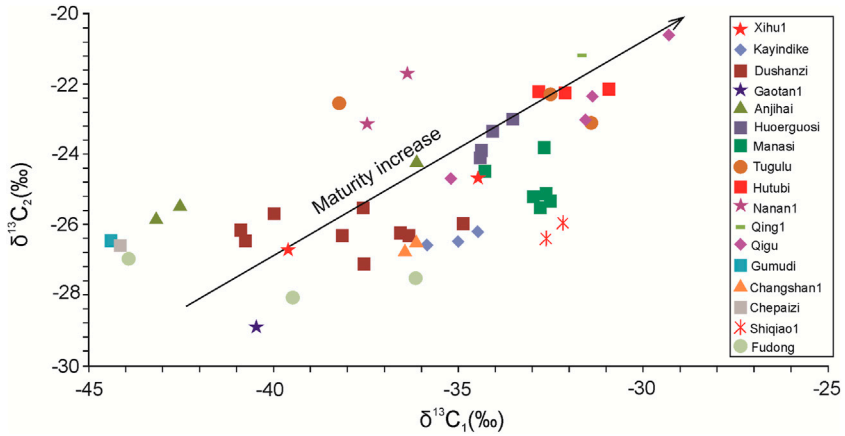

FIGURE 6 | Plot of $\delta^{13}C_1$ versus $\delta^{13}C_2$ for natural gas from the South Junggar foreland basin, showing gas derived from different maturity.

TABLE 1 | Input data and parameters used in the basin modeling.

Strata	Geological time (Ma)	Main Lithology	Main sedimentary faces	Thermal conductivity (W/m/K)	Average paleo surface temperature (°C)	Average paleo-water depth (m)	Average basal paleo heat flow (mW/m^2)
Q	1.65	Conglomerate	Piedmont-alluvial fan	2.93	15	0	40
N2d	5.2	Sandstone	Fluvial	2.78	14	5	41.5
N1t	16.3	Sandstone and silty sandstone	Fluvial-floodplain	2.65	14.95	12	42.0
N1s	23.3	Sandstone	Fan delta-shore	2.78	19.1	15	42.5
E2-3a	35.4	Mudstone	Shallow lake	2.05	19.6	20	43.0
E1-2z	65	Sandstone and mudstone	Alluvial fan	2.65	21.99	15	43.2
K2d	97	Siltstone	Fan delta-shore	2.97	23.2	20	43.5
K1tg	145	Mudstone and siltstone	Shallow-deep lake	2.01	22.1	45	46
J2-3	166	Sandstone	Alluvial fan-braided river	2.78	19	10	47.5
J1-2	208	Shale, siltstone, and coal	Braided river-shore, swamp	2.05	14.5	25	50
T	245	Sandstone and siltstone	Fluvial, alluvial fan	2.97	14	10	51.00

still exists about the origin of Type IV oil. Chen et al. (2016) concluded that it was sourced from $E_{2-3}a$ source rocks, whereas other studies considered that the low-mature $E_{2-3}a$ source rocks could not have provided such large volumes of oil and that the oil was sourced from Jurassic source rocks and mixed with Paleogene oil (Li et al., 2003; Guo et al., 2005).

The natural gas has a dry coefficient (C_1/C_{1-5}) of 0.72–0.99, $\delta^{13}C$ = −46.46 to −25.59‰ (generally < −29.29‰), and $\delta^{13}C_2$ = −30.03 to −20.60‰ (generally > −28‰) (**Figure 6**). The methylcyclohexane coefficient of the light hydrocarbon is >50, which reflects a coal-type origin, possibly from Jurassic coal measures. Compared with the oils, the origin of natural gas is relatively simple. Natural gas accumulation is widespread in the basin, such as in the Manasi, Hutubi, Huoerguosi, and Qigu anticlines. The carbon isotope data indicate that the maturity of the natural gas in the SJFB is not high and is mainly in the low-mature to mature stage, (**Figure 6**).

3 BASIN MODELING METHODOLOGY AND PARAMETERS

Basin modeling is a powerful tool for the evaluation of temperature, source rock maturity, and petroleum generation and migration in sedimentary basins (Tissot et al., 1987; Welte and Yalçin, 1988; Ungerer et al., 1990). We used the PetroMod® software package of IES, Germany, to undertake such modeling. This model is based on physical and chemical parameters that control the formation of commercial hydrocarbon accumulations in a sedimentary basin, which are deposition, compaction, heat transfer, hydrocarbon generation, and multiphase fluid flow (Ungerer et al., 1990; Thomas and Kauerauf, 2009).

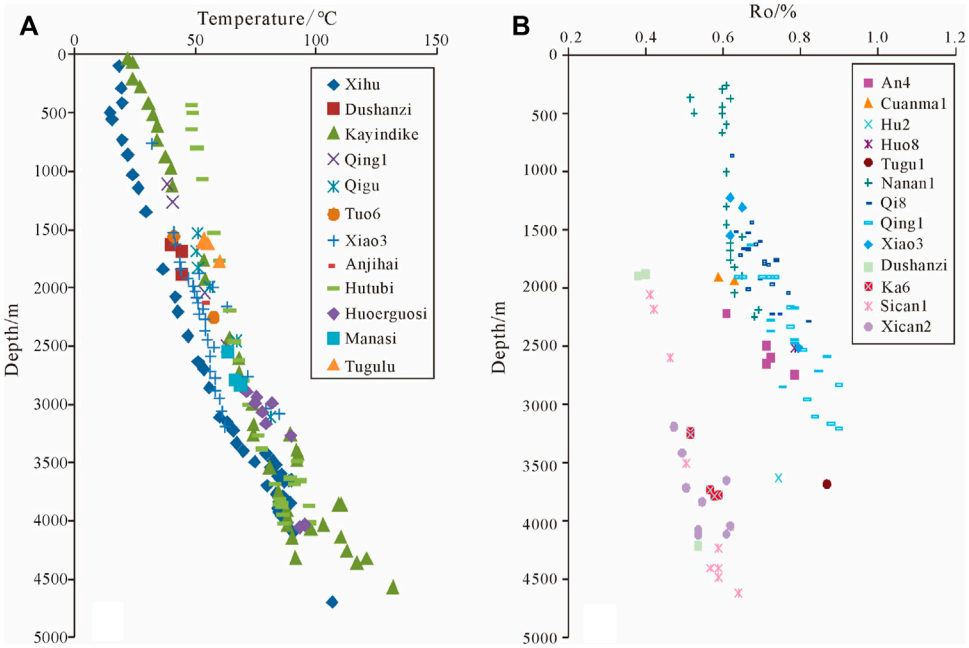

FIGURE 7 | Measured temperature and source rock Ro in different wells in the South Junggar Basin. **(A)** Measured temperature in different wells and structures in the south Junggar Basin. **(B)** Measured source rock Ro in different wells and structures in the south Junggar Basin.

For modeling, the input data were obtained from stratigraphic data (**Table 1**). Stratigraphic thicknesses and lithologies were extracted from well reports, and the petrophysical properties of the various lithologies were provided by the modeling package (**Table 1**). The paleo-surface temperature was estimated following the method of Wygrala (1989), based on the relationship between paleo-surface temperature and geological time and latitude. The transient heat flow method was used in the thermal modeling, and the Easy%Ro method was used in the source rock modeling. The basement heat flow data were taken from Rao et al. (2013) and adjusted by single-well 1D modeling with measured temperature and Ro data.

For the reason that the minor measured source rock Ro data are only distributed in the piedmont zone and the west slope of the Sikeshu depression (**Figure 7**), we combined multiple-well 1D modeling and 3D basin modeling to get a source rock maturity map. The single-well 1D modeling with measured temperature and Ro data provides the suggested modeling parameters, especially heat flow and erosion thickness. Then, a simple 3D model was established based on the thickness maps of each formation and the heat flow map is referred according to the previous work on heat flow distribution in the Junggar basin (Rao et al., 2013) but adjusted a little according to single-well modeling parameters. After 3D modeling, the results are rechecked with measured data. By using the advanced "Block" function, the 2D modeling of complicated compressional structural sections has been successfully carried out.

According to field measurements, the heat flow in the Junggar Basin is 23.4–56.1 mW/m^2, with an average of 42.5 ± 7.4 mW/m^2. This shows that the Junggar Basin is a typical cold basin. The heat flow is lower in the SJFB, with an average of 34.4 ± 8.3 mW/m^2. The geothermal gradient in the SJFB is as low as 1.5–2.2°C/100 m and is generally <1.8°C/100 m (**Figure 7**). This may be related to the rapid subsidence and burial history since the Cretaceous. Based on single-well modeling, the paleo-heat flow in the SJFB has declined since the Triassic, with the decrease being the largest in the Triassic–Jurassic (rifting and depression formation stage) and Neogene (rapid foreland deposition stage). Presently, the average heat flow is 40 mW/m^2 and varies from 35 to 42 mW/m^2 (**Table 1**).

Eight-well 1D modeling with measured temperature and Ro data was taken such as Xihu 1, Ka 6, Gaoquan 1, Dafeng 1, Qi 8, Qing 1, and Pencan 2 wells. The consistency between modeled and measured temperature and source Ro data in Xihu 1 and Qi 8 well is shown in **Figure 8**.

4 MODELING RESULTS AND DISCUSSION

4.1 Burial and Evolution of Maturity in Different Regions

The burial and evolution of maturity are variable throughout the SJFB. A comparative analysis of the Wukui anticline zone, Sikeshu depression, Qigu fault–fold zone, and northern slope zone shows that the burial history of the SJFB can be classified into four types.

4.1.1 Type I: Late-Stage Uplift and Erosion

This burial history affected the piedmont belt of the SJFB. Type I involved relatively little subsidence and three periods of structural uplift in the end-Jurassic (145 Ma), Cretaceous (65 Ma), and

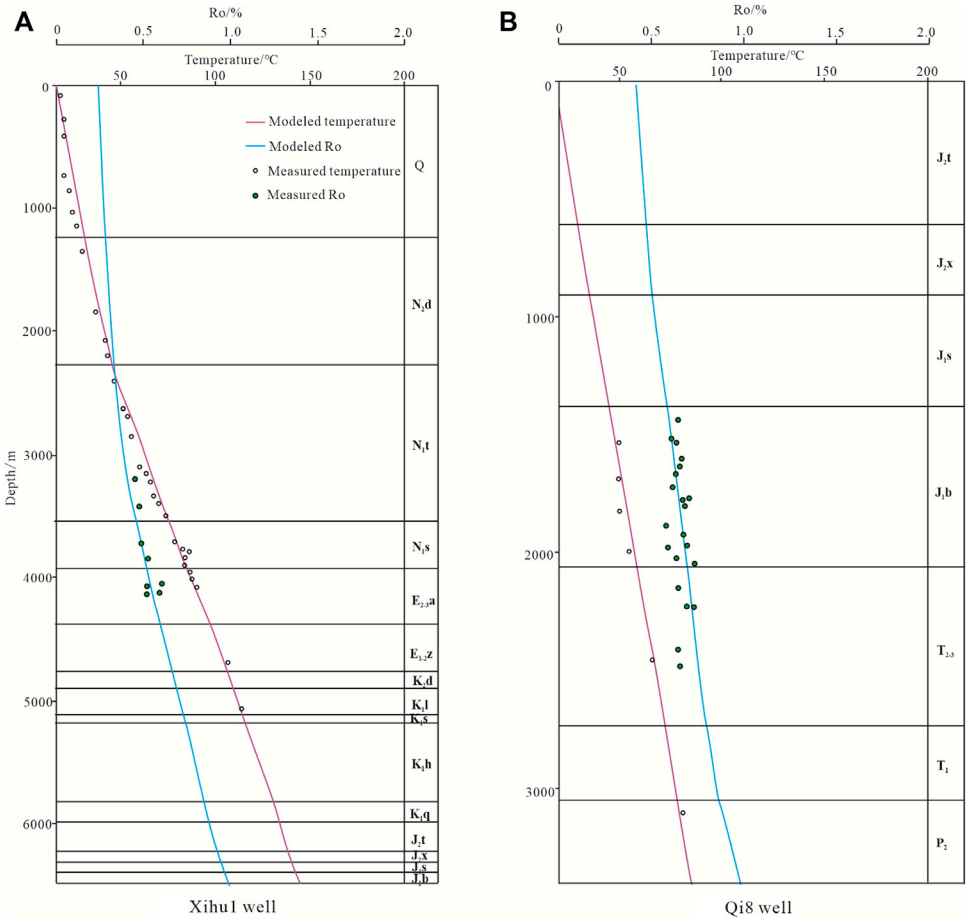

FIGURE 8 | Consistency between modeled and measured temperature and Ro in Xihu1 and Qi8 well. **(A)** Consistency between modeled and measured temperature and Ro data in Xihu1 well. **(B)** Consistency between modeled and measured temperature and Ro data in Qi8 well.

Miocene (17 Ma). The later period of uplift has largely shaped the region and has resulted in 2,000–3,000 m of uplift and further erosion (**Figure 9A**). The modeling of the Qi 8 well shows that the Ro values of the Permian source rocks reached 0.7% in the Late Jurassic and 0.9–1.0% in the Late Cretaceous, which then resulted in large amounts of oil generation. However, the end-Cretaceous uplift and erosion caused hydrocarbon generation to stop, and even the deposition of Cenozoic strata did not change the maturity of the Permian source rocks. The Ro values of Jurassic source rocks reached 0.5–0.6% in the Late Cretaceous but did not increase after end-Cretaceous uplift and erosion, thereby limiting oil generation.

4.1.2 Type II: Continued and Stable Burial

This burial history characterizes the second and third anticlinal belts in the middle segment of the SJFB. The burial was continuous and stable and has resulted in source rocks being buried to great depths and reaching high maturity (**Figure 9B**). The modeling of the Dafeng 1 well shows that multiple source rocks experienced a similar evolution and successive phases of hydrocarbon generation. The Permian source rocks entered the oil window during the Late Jurassic, and the oil generation peak was observed in the Cretaceous when Ro values reached 2.6%. Jurassic source rocks entered the oil window during the Early Cretaceous, later than the Permian source rocks, and were in the peak oil generation stage in the Late Cretaceous and gas generation stage since the Neogene. The Ro values are 2.3–2.6% and in the high- to over-mature stage. The Cretaceous source rocks entered the oil window during the Late Cretaceous, and peak oil generation has occurred since 10 Ma. Ro values reached 1.1%. The Ro values of the Paleogene source rocks are now 0.5%, and these rocks have not yet entered the oil window.

4.1.3 Type III: Early Shallow Burial and Late Rapid Burial

This burial history characterizes the Sikeshu depression and is involved in early shallow burial and later rapid burial. Although the rocks are currently deeply buried, the maturity is low. The modeling of the XH 1 well (**Figure 9C**) shows that in the Sikeshu depression, the burial depth of Jurassic source rocks was always <2,500 m prior to the Paleogene. Since the Paleogene, rapid burial

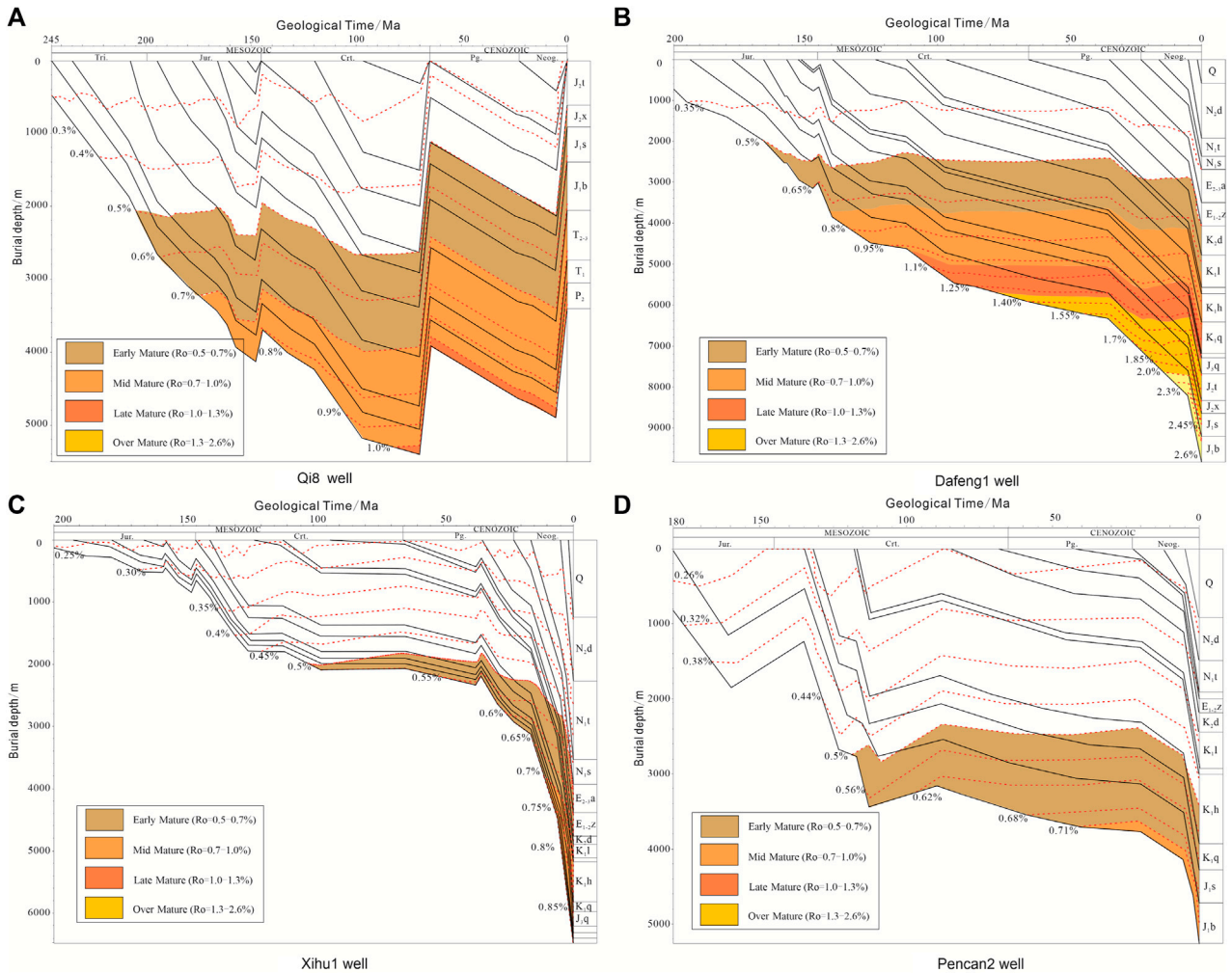

FIGURE 9 | Burial and thermal history of different regions in the South Junggar foreland basin. **(A)** Burial and thermal history of Qi8 well in the southern belt of anticlines showing late-stage uplift and erosion. **(B)** Burial and thermal history of Dafeng1 well in the northern belt of anticlines showing continued and stable burial. **(C)** Burial and thermal history of Xihu1 well in the Sikeshu depression, showing early shallow burial and late rapid burial. **(D)** Burial and thermal history of Pencan 2 well in the northern slope, showing continuous slow burial.

has occurred, but the low geothermal gradient means that Ro values of only 0.85–1.00% have been attained (i.e., oil generation stage). The Ro values of Cretaceous source rocks are <0.70% and are still not sufficient to generate large quantities of oil. The Ro values of the Paleogene source rocks are <<0.5%, outside of the oil generation stage.

4.1.4 Type IV: Continuous Slow Burial

This burial history is typical of the northern slope zone and is characterized by continuous slow burial. During the Cretaceous, the burial depth was <3,500 m, but this has increased since the Neogene, although it is still generally <5,000 m. The modeling of the Pencan 2 well (**Figure 9D**) demonstrates that the Jurassic source rocks in this area entered the oil window at the end-Early Cretaceous and, with the increase in burial depth since the Neogene, the Ro value has increased to 0.71%, which lies in the early oil generation stage. The *in situ* source rock maturity is low and has not yet generated a large amount of oil. The oil reservoirs in this area may be sourced from the adjacent depression or the SJFB.

4.2 Matching Between Trap Formation and HC Generation

Before the Cretaceous, the top structure of J_2x is a nearly EW-trending depression, shallow west, and deep east with steep south and gentle north. The first row of structures such as Changji and Qigu anticlines have formed, located in the southern steep slope edge area, and the western Tuositai area was also a large ancient trap. At the end of the Cretaceous, the west area of Shawan was a regional paleo-uplift, and the first row of the structural belt was also located in the southern margin, which was the direction area of oil and gas migration. Therefore, most of the structures in the SJFB did not form or only have prototypes in the Yanshan period,

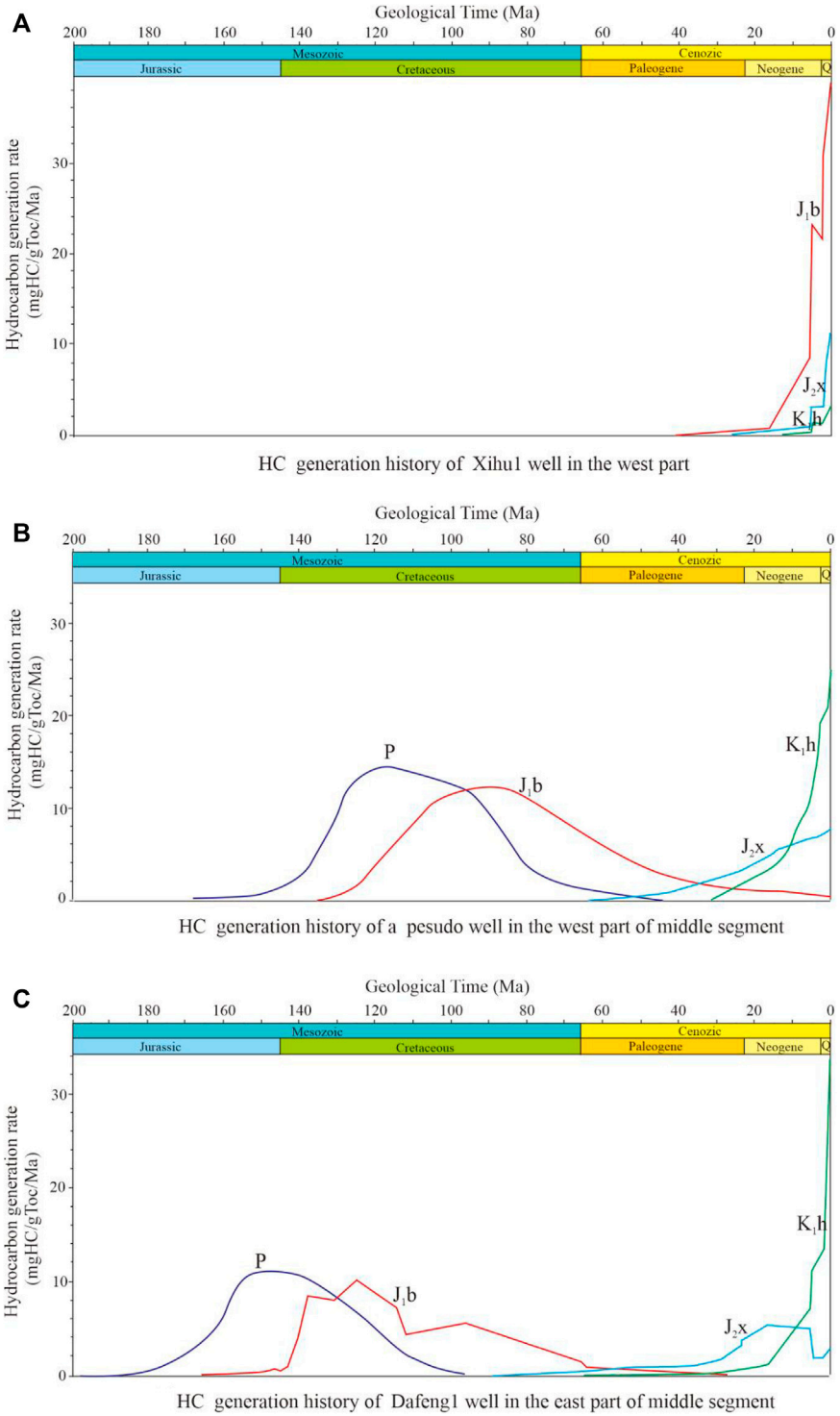

FIGURE 10 | Hydrocarbon generation history of representative wells in different regions in the Southern Junggar basin. **(A)** HC generation history of Xihu1 well in the west segment of south Junggar Basin. **(B)** HC generation history of a pseudo well in the west part of of middle segment. **(C)** HC generation history of Dafeng1 well in the east part of middle segment.

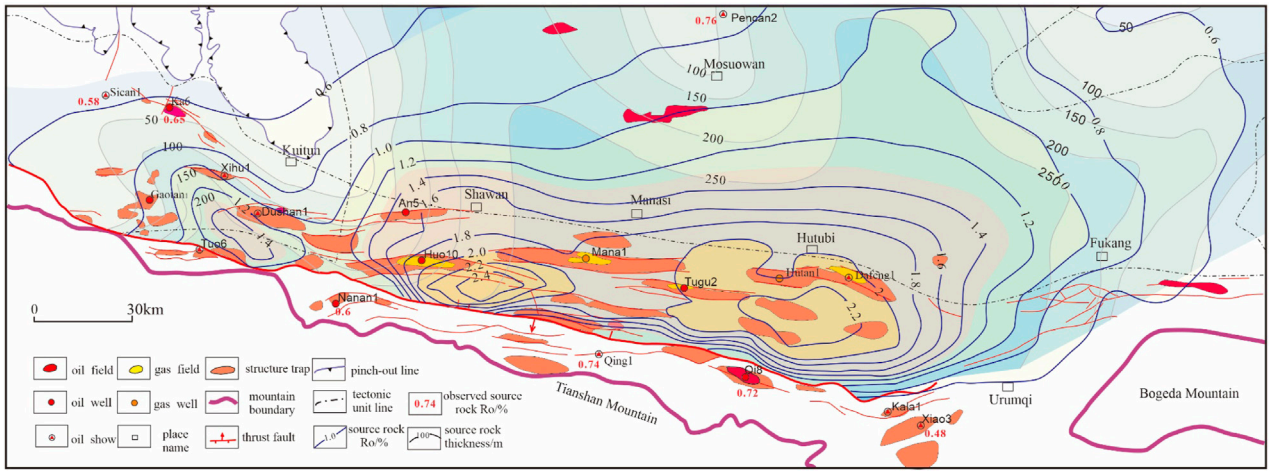

FIGURE 11 | Map showing the Jurassic source rock maturity and distribution of oil and gas in the South Junggar foreland basin. The measured Ro of some wells is shown in the map.

and the Himalayan period is the main formation period of structural traps. For the first row of anticlines, the trap is mainly formed in the Yanshan period, and it is reformed and finalized in the Himalayan period, which is well-matched with the hydrocarbon expulsion period of the source rock of the Middle and Lower Jurassic and is beneficial to the primary reservoir formation. The traps in the second and third row of anticlines are mainly formed in the Himalayan period, and the formation of traps is late, which does not match the hydrocarbon generation and expulsion period of main source rocks and is not conducive to the formation of primary reservoirs. According to the growth strata of anticlines, the formation or the stereotype time of the first row of anticlines is about 6–7 Ma, the second row of anticlines (Huo-Ma-Tu fold belt) is later than 2 Ma, and the third row of anticlines (Dushanzi-Anjihai fold belt) is not earlier than 1 Ma, which makes the formation time of structural traps generally prolonged than the main hydrocarbon generation period of oil and gas and may cause low oil and gas filling intensity, which may be one of the important reasons for the poor exploration effect of the southern Junggar thrust belt (Guo et al., 2011).

The study on the hydrocarbon generation history shows that the oil generation peak of the Middle–Lower Jurassic in the eastern part of the middle segment (take Dafeng 1 well as a representative) reached the peak of oil generation in the Cretaceous. The main hydrocarbon expulsion period should be at the end of the Cretaceous, and a large number of gas generation periods have entered since the Paleogene. The gas generation peak has reached around 20 Ma, but the hydrocarbon generation rate has decreased to around 10 Ma (**Figure 10C**). As for the late structure trap formation, it is not so favorable for oil and gas reservoir accumulation.

The eastern part of Sikeshu sag (take Xihu 1 well as a representative) has a burial history of early shallow burial and late fast deep burial. The Jurassic source rocks began to produce a large amount of oil since 10 Ma and are still involved in a large number of oil generation stages (**Figure 10A**), which is well-matched with the trap formation period and has the basic conditions for the formation of oil and gas fields. Early discovery has been found in the Caindike and Dushanzi oilfields, and the Xihu 1 well also had low-yield oil flow. In January 2019, the Gaotan 1 well had high-yield oil and gas flow in the K_1q reservoir, with a daily yield of crude oil of 1,213 m^3 and of natural gas 3,217,000 m^3.

As for the west part of the middle segment (take a pseudo well for modeling), due to the relatively shallow burial in the early stage, the hydrocarbon generation time is relatively lagging, and the Jurassic source rocks are still generating a lot of gas since 10 Ma (**Figure 10B**). The main gas generation period is better-matched with the late trap formation period. The area of Ro between 1.0 and 2.0% in the J1b source rock can be considered the main gas-generating area and is mostly distributed in the western and middle part of the middle segment of the fold-and-thrust belt, which has a good matching relationship with the formation period of structural traps and is a favorable exploration area for natural gas (**Figure 11**).

4.3 Source Rock Controls on the Hydrocarbon Phase and Distribution

Four sets of source rocks are present in the SJFB. Given that the Ro values of Paleogene source rocks are generally <0.6%, these rocks have made a negligible contribution to oil and gas generation and accumulation. The Cretaceous source rock in the middle segment has just gone into the middle mature stage, with an Ro of 0.8–1.1% (**Figure 12**), which will generate less oil, which has proven to be the source of oils in the Neogene and Cretaceous in Huoerguosi, Manasi, Tugulu, and Hutubi anticlines; however, it is limited both in area and quantity. The Permian source rocks generated

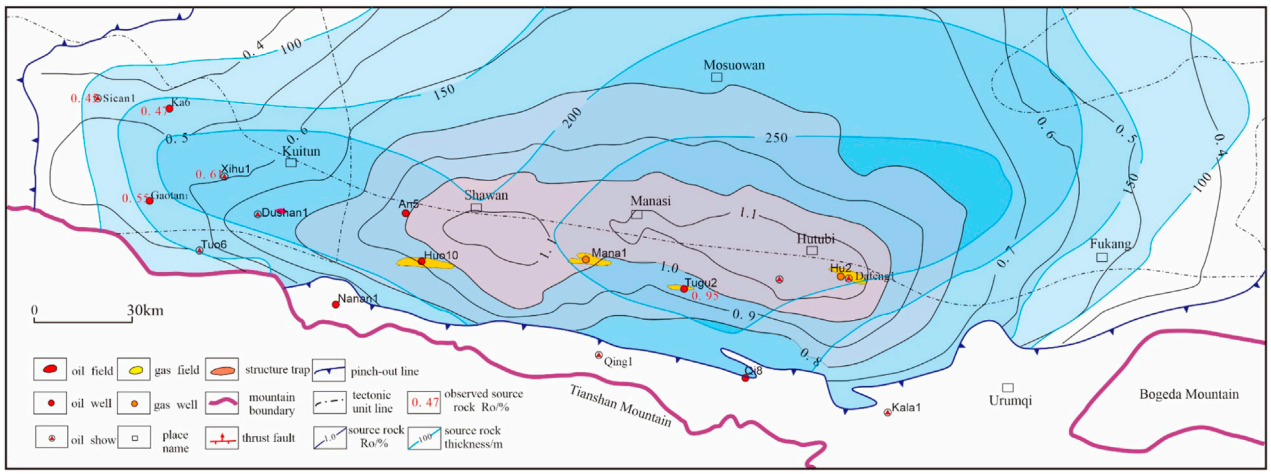

FIGURE 12 | Map showing the Cretaceous source rock maturity and thickness in the South Junggar Basin. The measured Ro of some wells is shown in the map.

TABLE 2 | Gas composition and carbon isotope in the South Junggar Basin.

Structure	Well no.	Formation	depth/m	Reservoir phase	C1/ %	C2+/ %	C1/ C1-5	N2/ %	δ13C1/ ‰	δ13C2/ ‰	δ13C3/ ‰	δ13C4/ ‰	Ro% of gas
Xihu	Xihu1	J3q	6,139–6,160	Oil	90.46	4.18	0.956	5.29	−39.68	−26.76			0.77
Gaoquan	Gaotan1	K1q	5,768–5,775	Oil	74.44	24.52	0.75	0.71	−40.35	−28.74	−26.54	−26.21	0.74
Kayindike	Ka6	J3q	3,956–3,980	Oil	81.33	13.3	0.83	4.83	−42.14	−29.74	−26.35		0.68
Dushanzi	Du53	N1	673–709	Oil	79.2	19.96		0.84	−40.85	−26.21	−22.46	0.00	0.73
Anjihai	An4	N1s	2,080–2,187	Oil					−43.15	−25.82	−23.44	−23.60	0.65
Huoerguosi	Huo001	E1-2z	2,936–2,940	Condensate gas					−33.50	−23.01	−23.00		1.14
Manasi	Mana1	E1-2z	2,557–2,561	Condensate gas	93.26		0.96		−32.60	−25.12	−22.53		1.25
Tugulu	Tu001	E1-2z	1,698–1,729	Condensate gas	87.49	4.49	0.916	3.25	−32.45	−22.34	−23.64		1.27
Hutubi	Hu001	E1-2z	3,584–2,590	Condensate gas	92.98	3.85	0.9458	1.69	−32.07	−22.27	−22.24	−22.73	1.32
Nananjihai	Nanan1	J1b	770–786	Oil	97.75	0.18	0.998	2.05	−37.51	−23.14			0.76
Qingshuihe	Qing1	J2x	2,642–2,361	Condensate gas					−31.61	−21.22	−22.32	−24.30	1.39
Qigu	Qi8	J1b	1,662–1,713	Oil	97.47	0.52	0.9823	0.72	−35.20	−24.69	−27.04	−28.27	0.96
Gumudi	Mu3	J2	529–532	Oil					−44.32	−26.52	−21.96		0.62
Changshan	Changshan1	J3q	1,178.2–1,268	Oil	86.92	11.77	0.885	1.23	−36.42	−26.72	−23.12		0.85
Chepaizi	Che82	J1b	3,063–3,080	Oil					−44.12	−26.63			0.62
Fudong	Fu1	J1b	3,130.9	Oil					−36.09	−27.55	−30.43		0.88

hydrocarbons early, prior to the formation of Cenozoic thrusting structures. The Jurassic source rocks are thick, widely distributed, moderately mature, and are therefore the main source rocks in the SJFB. This study now focuses on the Jurassic source rocks and their control on oil and gas distribution.

The Jurassic source rocks have the highest maturity in the Dafeng 1 well area (Ro = 2.2%) and lower maturity away from this region (**Figure 11**). In the eastern area of the middle segment, the Ro values are also high (≥1.8%). The source rocks in these areas are high to over-mature and mainly generate dry gas, which has accumulated in the Hutubi anticline, forming the Hutubi gas field. In the western area of the middle segment, the maturity is relatively low and Ro = 1.0–1.6%; the source rocks here have mainly generated oil and condensate gas. Mature gas from Jurassic source rocks has been found in the Huoerguosi, Manasi, Tugulu, and Anjihai oil fields, in the second and third anticlinal belts. In the western segment, Ro = 0.6–1.0%, which is at the low-mature to mature stage. This has generated oil that accumulated in the Dushanzi, Xihu, and Kayindike anticlines. Oil has been found in Jurassic reservoirs in the Xihu and Kayindike anticlines. In the

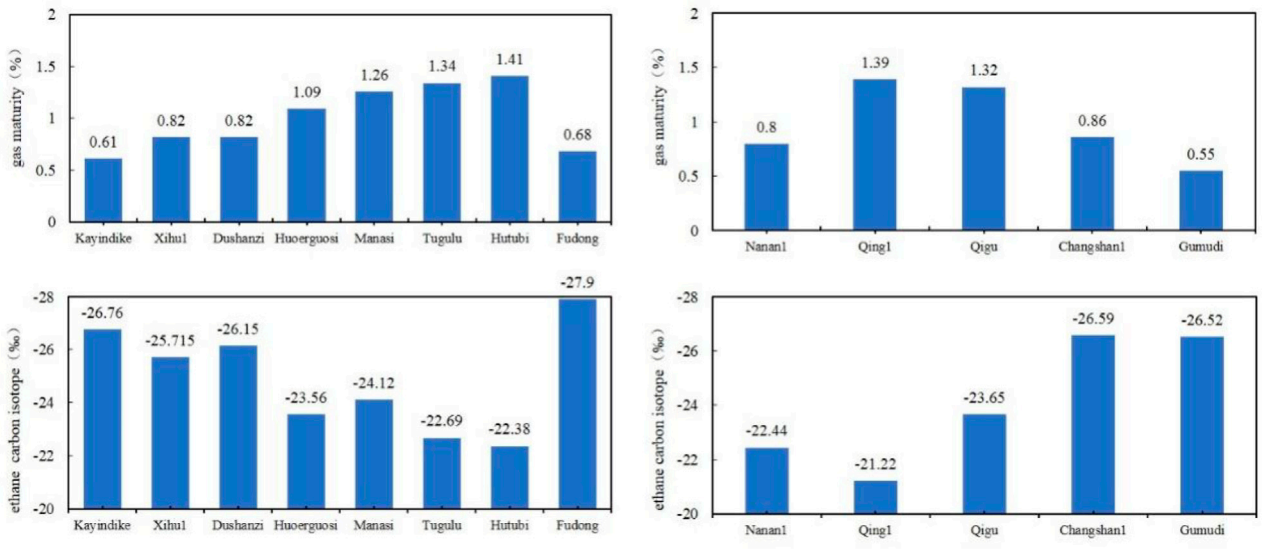

FIGURE 13 | East to west changes in carbon isotope data and natural gas maturity in the South Junggar foreland basin.

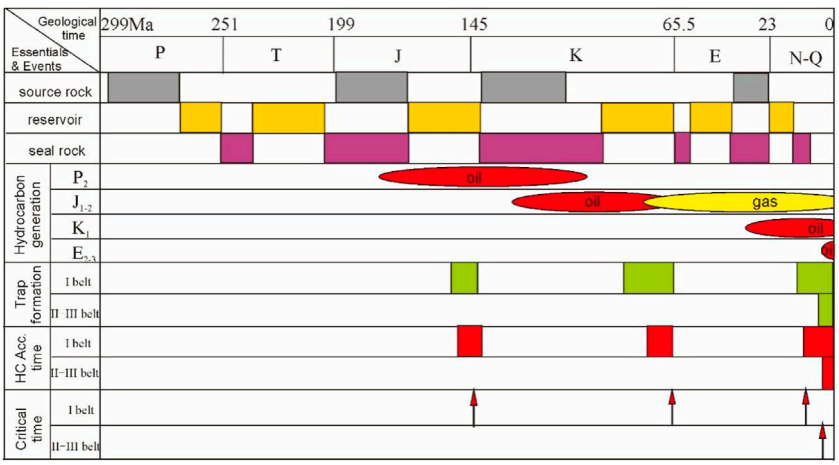

FIGURE 14 | Schematic diagram of hydrocarbon accumulation events in the South Junggar foreland basin. The four sets of source rock have different time for oil and gas generation and the different trap formation and hydrocarbon accumulation time between the first and second-third row of anticlines.

eastern segment, the source rock Ro values are relatively low (0.5–0.8%) and mainly generate oil. The Santai and Ganhezi oil fields have been found in the east piedmont belt.

The gas composition and carbon isotope and reservoir phase type in each discovered oil and gas field or well are listed in **Table 2**. The gas maturity is computed based on the linear relationship between methane carbon isotope and source rock Ro according to the type III source rock. The calculation formula is referred from the two-stage fitting mode of coal-derived gas after Liu and Xu (1999).

$$\delta^3C_1\,(‰) = 48.77\,\lg Ro - 34.1 \quad Ro < 0.8 \sim 1.0\%. \tag{1}$$

$$\delta^3C_1\,(‰) = 22.42\,\lg Ro - 34.8 \quad Ro < 0.8\%. \tag{2}$$

The Jurassic source rocks in the second and third anticlinal belts have the highest maturity, which has led to gas accumulation in the Huoerguosi–Manasi–Tugulu and Hutubi anticlines. These gases have heavy carbon isotopes and source rock Ro = 1.09–1.34%. The carbon isotopes of gas in the Qigu oil field and Qing 1 well are also heavy, and source rock maturity has reached Ro = 1.32–1.39% (**Figure 13**). The source rocks in the Sikeshu depression have low maturity because of the rapid subsidence, and Ro values are 0.6–0.8%, mainly resulting in oil and associated gas generation. The carbon isotopes of gas in the Kayindike, Xihu, and Dushanzi oil fields are light, and the source rocks have Ro = 0.61–0.82%. The source rock maturity is lowest in the eastern segment (Ro = 0.6%), and the source rocks have

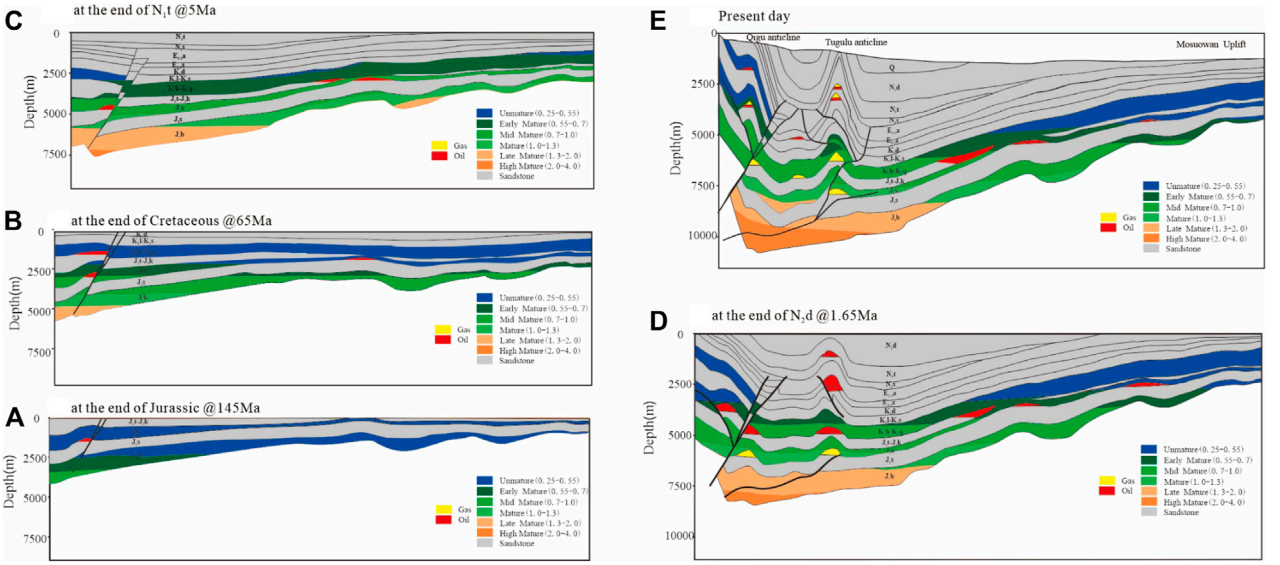

FIGURE 15 | Schematic diagram of tectonic deformation, source rock maturation, and hydrocarbon accumulation history in the middle segement of the South Junggar foreland basin. The structural and stratigraphy model is simplified from **Figure 3**. **(A)** The structure, source rock maturation and HC accumulation situation at the end of Jurassic at 145 Ma. **(B)** The structure, source rock maturation and HC accumulation situation at the end of Cretaceous at 65 Ma. **(C)** The structure, source rock maturation and HC accumulation situation at the end of N1t sedimentation at 5 Ma. **(D)** The structure, source rock maturation and HC accumulation situation at the end of N2d sedimentation at 1.65 Ma. **(E)** The structure, source rock maturation and HC accumulation situation at present day.

mainly generated oil. The carbon isotopes of reservoir-associated gas in the Gumudi and Fudong areas are the lightest in the SJFB, and the source rocks have Ro = 0.55–0.68%. From west to east, the source rock maturity first increases and then decreases, and the gas maturity changes in a similar fashion (**Figure 13**). This shows that source rock maturity largely controlled the oil and gas composition and phase. In general, oil and gas from Jurassic source rocks have resulted in gas accumulation in the middle segment, oil and gas accumulation in the western segment, and oil accumulation in the eastern segment. This spatial variability is controlled by source rock maturity.

4.4 Petroleum System Evolution

The composite petroleum systems of the SJFB have superimposed multiple sources, multiple phases of hydrocarbon generation, and multiple phases of (mixed) accumulation (Zhang and Liu, 2002; Zhao et al., 2009; Song et al., 2012) (**Figure 14**). The two N–S **section 2D** modeling results show the evolution of structure, source rock maturity, and hydrocarbon accumulation process, one in the middle segment (**Figure 15**) and one in the west segment (**Figure 16**), reflecting the difference between the west and middle segment and the first row and second-third row of anticlines.

In the Permian petroleum system, the main time of oil and gas generation was the Late Jurassic to Early Cretaceous, and hydrocarbon migration and accumulation occurred at the end-Jurassic. The favorable areas for accumulation are located in the Changji and Qigu anticlines in the piedmont belt because the paleo-structures in these areas had formed in the Late Jurassic. However, in the majority of the northern areas, Permian oil has migrated into uplifted areas of the northern slope zone along the tops of reservoirs.

In the Jurassic petroleum system, the source rocks in the middle segment began to generate oil in the Late Cretaceous and gas since the Neogene; the key times for hydrocarbon migration and accumulation were the end-Cretaceous and late Miocene–Pliocene (**Figures 14**, **15**). The primary oil reservoirs that are formed at the end of the Cretaceous are located in the first rows of anticlines. Given that the second and third row of anticlines had not yet formed in the Miocene–Pliocene, most of the Jurassic oil migrated toward the uplifted northern slope zone along the tops of reservoirs. As such, only lithological and structural–lithological reservoirs are formed in these zones. The second and third row of anticlines began to form in the late Miocene–Pliocene, and gas from the Jurassic source rocks migrated into the K_2d and $E_{1-2}z$ reservoirs along faults, forming late gas accumulations. The deep structural traps in the second and third rows of anticlines formed late, are not cut by faults, have good preservation conditions, and are ideal sites for hydrocarbon reservoirs. The Jurassic source rocks in the Sikeshu depression have generated the majority of their oil since the Neogene, with the key time of oil accumulation being in the late Miocene–Pliocene (**Figure 16**). Even though oil generation and accumulation are very late, the oil accumulations were adjusted a lot by the late Cenozoic tectonism, for example, the Xihu1 anticline was once a paleo oil reservoir, while producing less oil but much water at present.

In the Cretaceous petroleum system, the Cretaceous source rocks began to generate oil in the Neogene, and the

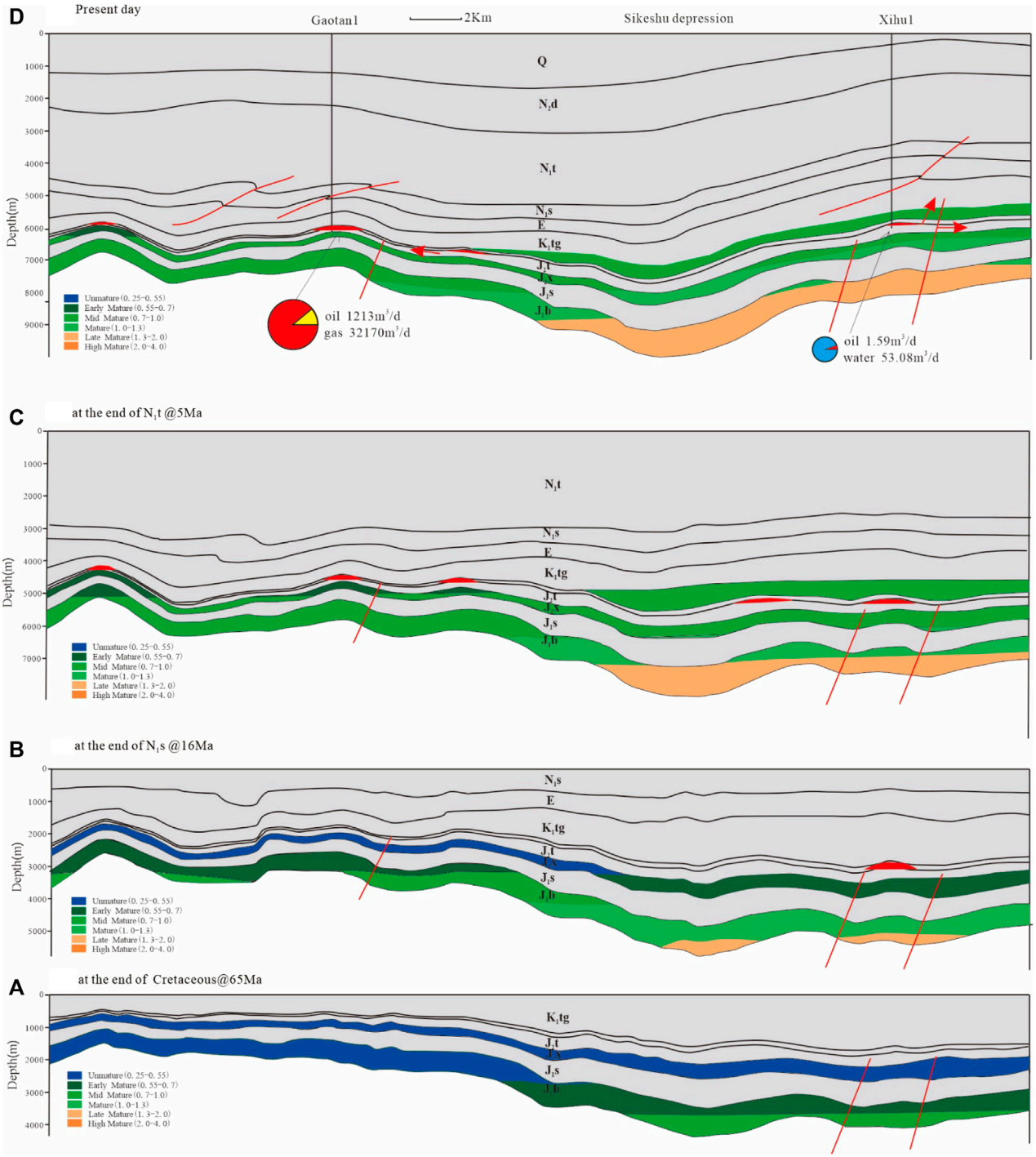

FIGURE 16 | Schematic diagram of tectonic deformation, source rock maturation, and hydrocarbon accumulation history in the west segment of the South Junggar foreland basin. The location of this section is shown in **Figure 1**. **(A)** The structure, source rock maturation and HC accumulation situation at the end of Cretaceous at 65 Ma. **(B)** The structure, source rock maturation and HC accumulation situation at the end of N1s sedimentation at 16 Ma. **(C)** The structure, source rock maturation and HC accumulation situation at the end of N1t sedimentation at 5 Ma. **(D)** The structure, source rock maturation and HC accumulation situation at present day.

key time for hydrocarbon migration and accumulation was during the deposition of N_2d (**Figures 14**, **15**). The Cretaceous oil migrated into the K_2d and E_{1-2}z reservoirs along the faults and charged the same traps with gas from the deeper Jurassic source rocks, forming condensate gas reservoirs by gas flushing. The favorable zones for these accumulations are in the Dushanzi, Huoerguosi, Manasi, and Tugulu anticlines.

Late Cenozoic tectonism has clearly controlled hydrocarbon accumulation in the SJFB. In the first row of anticlines, the hydrocarbons have multiple sources, a multistage accumulation history, and late overprints. Oil accumulation in the Qigu anticline began in the Late Jurassic (Song et al., 2005; Zhao et al., 2005; Fang et al., 2007; Wei et al., 2010), and high-mature gas accumulation occurred in the late Neogene (Zhao et al., 2005; Lu et al., 2019). In the second and third row of anticlines, hydrocarbon accumulation was delayed and has occurred since the Neogene (Hu et al., 2017). The Cretaceous source rocks have mainly generated oil, and the Jurassic source rocks have mainly generated gas. In the middle and upper structural layers, the faults have enabled the formation of mixed-source oil and gas reservoirs.

4.5 Petroleum Preferential Accumulation Sites

From our comprehensive analysis, it is evident that the distribution of source rocks in the petroleum systems has controlled the distribution of oil and gas reservoirs. Mixed accumulations were facilitated by fault connectivity. In the eastern segment, oil and gas reservoirs are found in Permian, Triassic, and Jurassic reservoirs sourced from P_2 and J_{1-2}. In the middle segment, oil and gas are mainly sourced from J_{1-2} and P_2 in lower reservoirs, such as in the Qigu oil field and the Nanan 1 well. However, oil is sourced mainly from K_1tg and gas from J_{1-2} *via* fault pathways in the middle–upper reservoir combinations, such as in the Hutubi gas and Manasi oil–gas fields. In the western segment, Cretaceous and Permian source rocks are not present, and oil and gas accumulated in Paleogene and Jurassic reservoirs, sourced mainly from J_{1-2} in lower reservoirs. However, oil and gas in the upper reservoirs are partly sourced from E_{2-3}a source rocks, such as in the Dushanzi oil field and the Kayindike E_{1-2}z oil reservoir.

Structural traps have good preservation conditions in the lower structural layer and have mainly accumulated gas. The times of oil and gas charging in the second row of anticlines were 14–9 and <3 Ma, respectively (Fang et al., 2007; Hu et al., 2017), corresponding to late Cenozoic tectonic activity. The northern slope zone is an area of long-term uplift and a favorable direction for oil and gas migration and subsequent accumulation, particularly for oil derived from Permian and Jurassic source rocks prior to the Neogene. The types of reservoirs in the northern slope zone are mainly lithological and structural–lithological.

5 CONCLUSION

1) There are four sets of source rocks in the SJFB, which are middle Permian, Middle–Early Jurassic, Early Cretaceous, and Paleogene in age. Middle–Lower Jurassic rocks are the main source rocks. These source rocks are vertically stacked and overlapped, forming a composite petroleum system, but the Jurassic petroleum system is dominant. The heterogeneous distribution of oil and gas reflects the variable source rock distribution and maturity, stratigraphy, relative timing of hydrocarbon generation, and formation of structural traps.
2) Multiple sources and multistage hydrocarbon charging have influenced the petroleum systems in the SJFB. Late Cenozoic structural deformation was also an important control on oil and gas accumulation. The timing of structural trap formation in the second and third row of anticlines was later than the main phase of hydrocarbon generation, which may explain the poor exploration outcomes in the SJFB.
3) According to our analysis of source rocks, reservoir–cap rock assemblages, and relative timing of hydrocarbon generation and trap formation, the lower reservoir-forming combination in the middle segment may contain large gas reservoirs with significant exploration potential. The conditions for hydrocarbon accumulation are most favorable in the second and third row of anticlines in the middle SJFB.

DATA AVAILABILITY STATEMENT

The original contributions presented in the study are included in the article/Supplementary Material; further inquiries can be directed to the corresponding author.

AUTHOR CONTRIBUTIONS

YL: methods and writing; XL: data and fund support; MZ: structure and data analysis; QZ: text typesetting and graphic drawing; LG: software.

FUNDING

This work is supported by the National Natural Science Foundation of China (No. 42172164 and No. 41902045), the Science Foundation of China University of Petroleum, Beijing (No. 2462020YXZZ022) and and PetroChina Science and Technology Project (No. 2021DJ0105 and No. 2021DJ0203).

ACKNOWLEDGMENTS

These sources of funding are gratefully acknowledged. We acknowledge the PetroChina Xinjiang Oilfield Company for their enthusiastic help and support by providing seismic profiles and drilling data.

REFERENCES

Avouac, J. P., Tapponnier, P., Bai, M., You, H., and Wang, G. (1993). Active Thrusting and Folding along the Northern Tien Shan and Late Cenozoic Rotation of the Tarim Relative to Dzungaria and Kazakhstan. *J. Geophys. Res.* 98 (B4), 6755–6804. doi:10.1029/92jb01963

Bullen, M. E., Burbank, D. W., Garver, J. I., and Abdrakhmatov, K. Y. (2001). Late Cenozoic Tectonic Evolution of the Northwestern Tien Shan: New Age Estimates for the Initiation of Mountain Building. *G. S A Bull. V.* 113 (12), 1544–1559. doi:10.1130/0016-7606(2001)113<1544:lcteot>2.0.co;2

Burchfiel, B. C., Brown, E. T., Qidong, D., Xianyue, F., Jun, L., Molnar, P., et al. (1999). Crustal Shortening on the Margins of the Tien Shan, Xinjiang, China. *Int. Geol. Rev.* 41, 665–700. doi:10.1080/00206819909465164

Charreau, J., Chen, Y., Gilder, S., Dominguez, S., Jean-Philippe, A., Sen, S., et al. (2005). Magnetostratigraphy and Rock Magnetism of the Neogene Kuitun He Section (Northwest China): Implications for Late Cenozoic Uplift of the Tianshan Moutains. *Earth Planet. Sci. Lett.* 230 (1-2), 177–192. doi:10.1016/j.epsl.2004.11.002

Charreau, J., Avouac, J.-P., Chen, Y., Dominguez, S., and Gilder, S. (2008). Miocene to Present Kinematics of Fault-Bend Folding across the Huerguosi Anticline, Northern Tianshan (China), Derived from Structural, Seismic, and Magnetostratigraphic Data. *Geol* 36 (11), 871–874. doi:10.1130/g25073a.1

Charreau, J., Chen, Y., Gilder, S., Barrier, L., Dominguez, S., Augier, R., et al. (2009). Neogene Uplift of the Tian Shan Mountains Observed in the Magnetic Record of the Jingou River Section (Northwest China). *Tectonics* 28, a–n. doi:10.1029/2007TC002137

Chen, J. P., Wang, X. L., and Deng, C. P. (2015a). Geochemical Feature of Source Rocks in the Southern Margin, Junggar Basin, Northwest China. *Acta Pet. Sin.* 36 (7), 767–780. doi:10.7623/syxb201507001

Chen, J. P., Wang, X. L., and Deng, C. P. (2015b). Geochemical Features and Classification of Crude Oil in the Southern Margin of Junggar Basin, Northwestern China. *Acta Pet. Sin.* 36 (11), 1315–1331. doi:10.7623/syxb201511001

Chen, J. P., Wang, X. L., and Deng, C. P. (2016). Investigation of Typical Reservoirs and Occurrence Regularity of Crude Oils in the Southern Margin of Junggar Basin, Northwestern China. *Acta Pet. Sin.* 37 (4), 415–429. doi:10.7623/syxb201604001

Chen, Z. L., Lu, K. G., and Wang, G. (2010). Characteristics of Cenozoic Structural Movement in Southern Margin of Junggar Basin and its Relationship to the Mineralization of Sandstone-type Uranium Deposits. *Acta Petrol. Sin.* 26 (2), 457–470.

Da, J., Song, Y., and Hong, F. (2006). Division of Hydrocarbon Accumulation System in the Southern Junggar Foreland Basin. *Nat. Gas. Geosci.* 17 (4), 567–585. doi:10.3969/j.issn.1672-1926.2006.04.003

Da, J., Song, Y., and Liu, S. B. (2007). Hydrocarbon Play and Controlling Factors in Fold-Thrust Belt of the Southern Junggar Foreland Basin. *Petroleum Geol. Exp.* 29 (4), 355–360. doi:10.1016/S1872-5813(07)60034-6

Deng, Q. D., Feng, X. Y., and Zhang, P. Z. (2000). *Active Tectonics of the Tian Shan Mountains*. Beijing: Seismological Press.

Du, J. H., Wang, Z. M., Hu, S. Y., Wang, Q. H., and Xie, H. W. (2012). Formation and Geological Characteristics of Deep Giant Gas Provinces in the Kuqa Foreland Thrust Belt, Tarim Basin, NW China. *Petrol Explor Dev.*. 39 (4), 385–393.

Fang, S. H., Jia, C. Z., Song, Y., and Guo, Z. J. (2007). Late Cenozoic Structural Deformation and its Implication for Petroleum Accumulation in the Southern Junggar Thrust Belt. *Acta Pet. Sin.* 28 (6), 1–5.

Guan, S., Joseph, M. S., Shaw, J. H., Plesch, A., and Jian, Z. (2016). Structural Inversion, Imbricate Wedding, and Out-Of-Sequence Thrusting in the Southern Junggar Fold-And-Thrust Belt, Northern Tianshan, China. *AAPG Bull.* 100 (9), 1443–1468. doi:10.1306/04041615023

Guo, C. Q., Shen, Z. M., Zhang, L. Y., and Lu, X. Y. (2005)., 32. China, 257–262.Biogenic Origin Characteristics of Hydrocarbon Source Rocks and Classification of Oils in the South Part of Junggar Basin*J. Chengdu Univ. Technol. Sci. Technol. Ed.*3

Guo, Z. J., Deng, S. T., Wei, G. Q., and Li, B. L. (2007). Comparative Study of the Foreland Thrust Belts of South and North Tianshan and Implications for Hydrocarbon Accumulation. *Earth Sci. Front.* 14 (4), 123–131. doi:10.1016/S1872-5791(07)60030-X

Guo, Z. J., Fang, S. H., Zhang, R., and Zhang, Z. (2006). Growth Strata and Their Application in Timing Deformation of Foreland Thrust-fold Belts in the North Margin of Tianshan. *Oil Gas Geol.* 27 (4), 475–481.

Guo, Z. J., Wu, C. D., Zhang, Z. C., and Chen, W. (2011). Tectonic Control on Hydrocarbon Accumulation and Prospect for Large Oil-Gas Field Exploration in the Southern Junggar Basin. *Geol. J. China Univ.* 17 (2), 185–195. doi:10.1007/s12182-011-0118-0

Hu, H., Zhang, J., Tian, X., Zhuo, Q., Jia, C., and Guo, Z. (2017). Evolution of the Deeply Buried Jurassic Reservoirs in the Southern Junggar Basin, NW China: Evidences from the Well DS-1. *Petroleum Res.* 2 (3), 247–263. doi:10.1016/j.ptlrs.2017.06.007

Jia, C. (2007). The Characteristics of Intra-continental Deformation and Hydrocarbon Distribution Controlled by the Himalayan Tectonic Movements in China. *Earth Sci. Front.* 14 (4), 96–104. doi:10.1016/s1872-5791(07)60030-x

Jia, C. Z. (2009). The Structures of Basin and Range System Around the Tibetan Plateau and the Distribution of Oil and Gas in the Tarim Basin. *Geotect. metallogenia* 33 (1), 1–9. doi:10.1016/S1874-8651(10)60080-4

Jia, C. Z., Wei, G. Q., and Li, B. L. (2005). Superimposed Composite Characteristics of Micro-carton Basins and its Bearing Petroleum Systems, Central-Western China. *Geol. J. China Univ.* 11 (4), 479–482. doi:10.1360/gs050303

Jia, C. Z., Yang, S. F., Wei, G. Q., Wang, L. S., and Liu, S. W. (2008). Structural Characteristics and Petroleum Bearing Prospects of Cenozoic Circum-Tibet Plateau Basin and Range System in China. *Oil Gas Industry* 28 (8), 1–11.

Kang, Y. Z. (2003). Oil and Gas Prospect in the Thrust Belt of Tian Shan in Junggar Basin. *Xinjiang Geol.* 21 (2), 163–166.

Kuang, J., and Jia, X. Y. (2005). Relationship between Himalayan Movement and Hydrocarbon Accumulation in Southern Margin of Junggar Basin. *Xinjiang Pet. Geol.* 26 (2), 129–133. doi:10.1111/j.1440-1789.2005.00601.x

Kuang, J., and Liu, D. G. (2001). Comparative Analysis on Natural Gas Reservoir-Formed Conditions between South Margin of Junggar Basin and Kuche Depression of Tarim Basin. *Xinjiang Pet. Geol.* 22 (4), 287–290.

Kuang, J., and Qi, X. F. (2006). The Structural Characteristics and Oil-Gas Explorative Direction in Junggar Foreland Basin. *Xinjiang Pet. Geol.* 27 (1), 5–9.

Li, B. L., Chen, Z. X., Lei, Y. L., and Zhang, C. J. (2011a). Structural Geology Correlation of Foreland Thrust-Folded Belts between the Southern and Northern Edges of the Tianshan Mountain and Some Suggestions for Hydrocarbon Exploration. *Acta Geol. Sin.* 32 (3), 395–403. doi:10.7623/syxb201103004

Li, B. L., Wei, G. Q., Jia, C. Z., Guan, S. W., and Shi, X. (2009). Some Key Tectonic Characteristics of Chinese Foreland Basins and Related Petroleum Geology. *Geoscience* 23 (4), 575–586.

Li, B., Song, Y., Meng, Z. F., and Xia, B. (2007). Hydrocarbon Accumulation Pattern and Type in the Southern Junggar Foreland Basin. *Petroleum Geol. Exp.* 29 (5), 452–461. doi:10.11781/sysydz200705452

Li, C., Dupont-Nivet, G., and Guo, Z. (2011b). Magnetostratigraphy of the Northern Tian Shan Foreland, Taxi He Section, China. *Basin Res.* 23, 101–117. doi:10.1111/j.1365-2117.2010.00475.x

Li, C., Guo, Z., and Dupont-Nivet, G. (2011). Late Cenozoic Tectonic Deformation across the Northern Foreland of the Chinese Tian Shan. *J. Asian Earth Sci.* 42, 1066–1073. doi:10.1016/j.jseaes.2010.08.009

Li, X. Y., Shao, Y., and Li, T. M. (2003). Three Oil Reservoir Combinations in South Marginal of Jungar Basin, Northwest China. *Petroleum Explor. Dev.* 30 (6), 32–34. doi:10.1007/BF02974893

Liu, H. F., Liang, H. S., Cai, L. G., Xia, Y. P., and Liu, L. Q. (1994). Evolution and Structural Style of Tianshan and Adjacent Basins, Northwestern China. *Earth Sci.* 19 (6), 727–741.

Liu, W. H., and Xu, Y. C. (1999). A Two-Stage Model of Carbon Isotopic Fractionation in Coal-Gas. *Geochimica* 28 (4), 359–366.

Lu, H., Burbank, D. W., Li, Y., and Liu, Y. (2010). Late Cenozoic Structural and Stratigraphic Evolution of the Northern Chinese Tian Shan Foreland. *Basin Res.* 22 (3), 249–269. doi:10.1111/j.1365-2117.2009.00412.x

Lu, H. F., Chen, C. M., Liu, Z. H., Jia, D., Wang, G. Q., and Jia, C. Z. (2000). The Structural Features and Origin of the Kuqa Rejuvenation Foreland Thrust Belt. *Acta Pet. Sin.* 21 (3), 18–24.

Lu, H. F., David, G. H., Jia, D., and Cai, D. S. (1994). Rejuvenation of the Kuqa Foreland Basin, North Flank of the Tarim Basin, Northwest China. *Int. Geol. Rev.* 36, 1151–1158. doi:10.1080/00206819409465509

Lu, X. S., Zhao, M. J., Chen, Z. X., Li, X. Y., Hu, H. W., and Zhuo, Q. G. (2019). Recognition of Hydrocarbon Accumulation in Qigu Oilfield and Implications for Exploration in the Southern Margin of Junngar Basin. *Acta Pet. Sin.* 40 (9), 1045–1058. 1115. doi:10.7623/syxb201909003

Molnar, P., and Tapponnier, P. (1975). Cenozoic Tectonics of Asia: Effects of a Continental Collision: Features of Recent Continental Tectonics in Asia Can Be Interpreted as Results of the India-Eurasia Collision. *Science* 189, 419–426. doi:10.1126/science.189.4201.419

Rao, S., Hu, S. B., Zhu, C. Q., Tang, X. Y., Li, W. W., and Wang, J. T. (2013). The Characteristics of Heat Flow and Lithospheric Thermal Structure in Junggar Basin, Northwest China. *Chin. J. Geophys.* 56 (8), 2760–2770. doi:10.6038/cjg20130824

Shaw, J. H., and Suppe, J. (1994). Active Faulting and Growth Folding in the Eastern Santa Barbara Channel, California. *Geol. Soc. Am. Bull.* 106, 607–626. doi:10.1130/0016-7606(1994)106<0607:afagfi>2.3.co;2

Song, Y., Fang, S. H., Zhao, M. J., and Liu, S. B. (2005). The Structural Segmentation of Foreland Thrust Belts and its Implications for Hydrocarbon Accumulation in Foreland Basins in Central and Western China. *Earth Sci. Front.* 12 (3), 31–38. doi:10.1016/j.molcatb.2005.02.001

Song, Y., Zhao, M. J., Fang, S. H., Xie, H. W., Liu, S. B., and Zhuo, Q. G. (2012). Dominant Factors of Hydrocarbon Distribution in the Foreland Basins, Central and Western China. *Petroleum Explor. Dev.* 39 (3), 265–274. doi:10.1016/s1876-3804(12)60044-5

Sun, J., Zhu, R., and Bowler, J. (2004). Timing of the Tianshan Mountains Uplift Constrained by Magnetostratigraphic Analysis of Molasse Deposits. *Earth Planet. Sci. Lett.* 219, 239–253. doi:10.1016/s0012-821x(04)00008-1

Suppe, J., Chou, G. T., and Hook, S. C. (1992). "Rates of Folding and Faulting Determined from Growth Strata," in *Thrust Tectonics [M]*. Editor K R McKlay (London: Chapman Hall Publisher), 105–121. doi:10.1007/978-94-011-3066-0_9

Tapponnier, P., and Molnar, P. (1979). Active Faulting and Cenozoic Tectonics of the Tien Shan, Mongolia, and Baykal Regions. *J. Geophys. Res.* 84, 3425–3459. doi:10.1029/jb084ib07p03425

Thomas, H., and Kauerauf, A. I. (2009). *Fundamentals of Basin and Petroleum Systems Modeling[M]*. Springer, 90–98.

Tissot, B. P., Pelet, R., and Ungerer, P. (1987). Thermal History of Sedimentary Basins, Maturation Indices, and Kinetics of Oil and Gas Generation. *AAPG* 71, 1445–1466. doi:10.1306/703c80e7-1707-11d7-8645000102c1865d

Ungerer, P., Burrus, J., Doligez, B., Chenet, P. Y., and Bessis, F. (1990). Basin Evaluation by Integrated Two-Dimensional Modeling of Heat Transfer, Fluid Flow, Hydrocarbon Generation, and Migration. *AAPG* 74, 309–335. doi:10.1306/0c9b22db-1710-11d7-8645000102c1865d

Wang, L., Liu, G. L., and Yu, B. (2007). Main Control Factors of Hydrocarbon Accumulation of the Fold-Thrust Zone in the Southern Junggar Foreland Basin. *J. Daqing Petroleum Inst.* 31 (5), 27–30.

Wang, X., Jia, C. Z., and Yang, S. F. (2002). Geometry and Kinematics of the Kuqa Fold-and-Thrust Belt in the Southern Tianshan: Progress in Geophysics 32 (02), 1308–1313.

Wei, D. T., Zhao, Y. C., Abulimit, C. T., Yang, H. B., Wu, L. Y., and Li, S. H. (2010). Difference of Hydrocarbon Accumulation in the Foreland Thrust-fold Belt of the Southern Junggar Basin. *Geol. J. China Univ.* 16 (3), 339–350. doi:10.3724/SP.J.1231.2010.06586

Welte, D. H., and Yalçin, M. N. (1988). Basin Modelling-A New Comprehensive Method in Petroleum Geology. *Org. Geochem.* 13 (1-3), 141–151. Xiao L.X., Lei D.W., Wei L.Y. doi:10.1016/0146-6380(88)90034-4

Xiao, A. C., Wu, L., Li, H. G., and Wang, L. Q. (2013). Tectonic Processes of the Cenozoic Altyn Tagh Fault and its Coupling With the Qaidam Basin, NW China. *Acta Petrologica Sinica* 29 (8), 2826–2836.

Yin, A., Nie, S., Craig, P., Harrison, T. M., Ryerson, F. J., Qian, X., et al.(1998). Late Cenozoic Tectonic Evolution of the Southern Chinese Tian Shan. *Tectonics* 17, 1–27. doi:10.1016/b978-0-08-037236-5.50020-8

Yu, F. S., Li, G. Z., and Yang, G. D. (2009). Deformation Feature and Genesis Simulation of Fold and Thrust Belts in the Southern Margin. *Junggar basin Geotect. metallogenia* 33 (3), 386–395. doi:10.1016/S1874-8651(10)60080-4

Zhang, P. Z., Deng, Q. D., and Yang, X. P. (1996). Late Cenozoic Tectonic Deformation and Mechanism along the Tianshan Mountain, Northwestern China. *Earthq. Res. China* 12 (2), 127–140. doi:10.1007/BF02974893

Zhang, Y. J., and Liu, G. D. (2002). Characteristics and Evolution of Composite Petroleum Systems and the Exploration Strategy in Junggar Basin, Northwest China. *Petroleum Explor. Dev.* 29 (1), 36–39.

Zhao, M. J., Lu, X. S., and Zhuo, Q. G. (2015). Characteristics and Distribution Law of Hydrocarbon Accumulation in Kuqa Foreland Basin. *Acta Pet. Sin.* 36 (4), 395–404. doi:10.7623/syxb201504001

Zhao, M. J., Song, Y., and Liu, S. B. (2009). Accumulation Systems and Filling Process of Natural Gas in Junggar Basin. *Geol. Rev.* 55 (2), 215–224. doi:10.1016/S1874-8651(10)60080-4

Zhao, M. J., Song, Y., and Qin, S. F. (2005). The Multi-Stage Formation of Oil-Gas Pools and Late-Stage Accumulation of Gas in the Foreland Basins in Central and Western China. *Earth Sci. Front.* 12 (4), 525–533.

Conflict of Interest: LX, ZM, ZQ, and GL were employed by PetroChina. LX, ZM, ZQ, and GL were employed by CNPC. CNPC provided data for the study and China University of Petroleum (Beijing) provided methods and writing.

The remaining author declares that the research was conducted in the absence of any commercial or financial relationships that could be construed as a potential conflict of interest.